Ecological Monographs, 65(3), 1995, pp. 261–281

NONLINEAR DEMOGRAPHIC DYNAMICS: MATHEMATICAL MODELS, STATISTICAL METHODS, AND BIOLOGICAL EXPERIMENTS[1]

BRIAN DENNIS
Department of Fish and Wildlife Resources, University of Idaho, Moscow, Idaho 83844 USA

ROBERT A. DESHARNAIS
Department of Biology, California State University, Los Angeles, California 90032 USA

J. M. CUSHING
Department of Mathematics, University of Arizona, Tucson, Arizona 85721 USA

R. F. COSTANTINO
Department of Zoology, University of Rhode Island, Kingston, Rhode Island 02881 USA

Abstract. Our approach to testing nonlinear population theory is to connect rigorously mathematical models with data by means of statistical methods for nonlinear time series. We begin by deriving a biologically based demographic model. The mathematical analysis identifies boundaries in parameter space where stable equilibria bifurcate to periodic 2-cycles and aperiodic motion on invariant loops. The statistical analysis, based on a stochastic version of the demographic model, provides procedures for parameter estimation, hypothesis testing, and model evaluation. Experiments using the flour beetle *Tribolium* yield the time series data. A three-dimensional map of larval, pupal, and adult numbers forecasts four possible population behaviors: extinction, equilibria, periodicities, and aperiodic motion including chaos. This study documents the nonlinear prediction of periodic 2-cycles in laboratory cultures of *Tribolium* and represents a new interdisciplinary approach to understanding nonlinear ecological dynamics.

Key words: bifurcation analysis; chaos; cycles; equilibrium; hypothesis testing; model evaluation; nonlinear demographic dynamics; parameter estimation; stability; Tribolium.

INTRODUCTION

Understanding the complex fluctuations in animal population numbers has far-reaching applications in areas ranging from food production to the conservation of species diversity. The hypothesis that the fluctuations are the result of nonlinear dynamic forces has proved to be elusive to test due to the difficulties of gathering adequate ecological data, of experimentally manipulating ecological systems, and of evaluating complex mathematical models with ecological data (Bartlett 1990, Costantino and Desharnais 1991, Logan and Hain 1991, Logan and Allen 1992, Hastings et al. 1993). Our approach to testing population theory is to connect rigorously a nonlinear demographic model with biological data by means of newly developed statistical methods for nonlinear time series.

Nonlinear demographic models were introduced along with the more familiar linear matrix models (Leslie 1948). Since that time, many density-dependent models have been studied (see Cushing 1988, Caswell 1989, and references therein). Linear models yield exponential growth whereas nonlinear models have the potential for more complex dynamical behaviors including periodic and aperiodic cycles and chaos. Some of the earliest examples of chaotic dynamics were recognized in ecological models (May 1974*a*). The detection of these more complex dynamics is an area of active research. Schaffer (1984, 1985) and Schaffer and Kot (1985, 1986*a*, *b*) emphasized the important role of chaos in ecology. Alternatives to Schaffer and colleagues' geometrical analyses (Takens 1980) include response surface methodology (Turchin and Taylor 1992, Turchin 1993) and model-free methods of estimating Lyapunov exponents in a time series with nonparametric regression (Ellner et al. 1991, McCaffrey et al. 1992).

The approach here begins with the construction of a biologically based dynamical model. Analytical and numerical methods are used to gain a mathematical understanding of the dynamical behavior predicted by the model. A key aspect of connecting model with data is the reformulation of the model in stochastic terms, which provides an explicit likelihood function for statistical estimation and testing. The nonlinear mathematical model then becomes a vulnerable scientific hypothesis that can be confronted by data.

The working hypothesis in the present study is that the dynamics of cultures of the flour beetle *Tribolium* can be explained by a mechanistic biologically based system of nonlinear difference equations. The mathe-

[1] Manuscript received 18 January 1994; revised 8 August 1994; accepted 11 October 1994; final version received 21 November 1994.

matical analysis of the model involves a study of the equilibrium states and their stability and a bifurcation study of nonequilibrium states. This analysis identifies boundaries in parameter space where stable equilibria bifurcate to 2-cycles and aperiodic motion on invariant loops. The statistical analysis is based on a stochastic version of the demographic model. This analysis provides procedures for parameter estimation, hypothesis testing, and model evaluation. The biological experiments yield the time series data. Statistical inference methods are applied to these data to estimate model parameters and evaluate model predictions. In so doing we locate the biological population in model parameter space and identify the type of dynamical behavior displayed by the population.

Mathematical Model

Biologically based dynamical model

The *Tribolium* system possesses great potential for the experimental study of nonlinear dynamics (Costantino and Desharnais 1991). The combination of (1) high reproductive rates, (2) short life cycle (4 wk from egg to adult), (3) ease of culture, (4) accurate censusing of all life stages, and (5) the complexities of metazoan life history that include strong nonlinear life stage interactions, make it a good laboratory system. In particular, some species of *Tribolium* are cannibalistic (Park et al. 1965). Adults feed on eggs, larvae, pupae, and callows (young adults) while larvae eat eggs, pupae, and callows. Neither larvae nor adults eat mature adults and larvae do not feed on larvae. Although not biologically complete, an approximation to a particular cannibalistic interaction can be described easily. Consider a group of L_t feeding larvae. Assume that a larval–egg contact means that the egg is eaten and also that the contacts are randomly distributed among the eggs. The probability of an egg not being eaten is computed using the binomial distribution as $(1 - c_{el})^{L_t} \approx \exp(-c_{el}L_t)$ where c_{el} is the coefficient of larval cannibalism on eggs. Dynamic complexity arises from these many nonlinear behavioral interactions.

We propose a model with three state variables corresponding to three functional life stages: feeding larvae, denoted by L_t, last instar (nonfeeding) larvae, pupae, and callow adults, denoted by P_t, and mature adults, denoted by A_t. We will refer to these state variables for convenience as "larvae," "pupae," and "adults" throughout this paper, but we will be careful to draw distinctions where confusion might arise. Published data on the feeding behavior of *Tribolium* larvae are scarce, but the results of Park et al. (1965: Table 10) for *T. castaneum* suggest that 14 d is a reasonable estimate of the feeding larva stage duration. More information is available on developmental periods; Moffa and Costantino (1977: Table 1) estimate a time from egg to adulthood of ≈27 d for the corn oil sensitive strain of *T. castaneum*. The 27 d include 2–4 d in the egg stage, but an additional 2–4 d are spent as a callow adult. Thus, the durations of the first two stages are roughly identical, ≈14 d under standard laboratory conditions. We exploit the coincidence of the two-stage developmental times by taking the unit of time in the model between censuses to be 2 wk.

We omitted an egg stage from the model. Though eggs can be and are sometimes counted in flour beetle studies, an inordinate amount of time is required to separate eggs from the media. Counting just larvae, pupae, and adults allows many more cultures to be maintained in a given experiment. The egg stage is fairly short in duration, ≈4 d (Sokoloff 1974), and so most eggs laid within a 2-wk period become larvae by the end of the period.

Larvae are thus the stage being recruited in the model. Recruitment of larvae at time t is assumed to be proportional to the number of adults at time $t - 1$. The assumption potentially introduces some bias in the model predictions in that a limited number of eggs laid just prior to time $t - 1$ can in reality be present in the larval class at time t; adults at time $t - 2$ have some limited contribution to larval recruitment at time t. However, our hypothesis is that the effect of A_{t-2} on larval recruitment at time t is slight compared to the effects of other factors (namely, A_{t-1} through egg-laying and cannibalism and L_{t-1} through cannibalism). Whether or not our model can account for a substantial portion of the dynamics of the system is a question we address later with data (see *Biological experiments* section below).

The model, which we term the "LPA model," is a system of three difference equations:

$$L_{t+1} = bA_t\exp(-c_{ea}A_t - c_{el}L_t), \quad (1)$$

$$P_{t+1} = L_t(1 - \mu_l), \quad (2)$$

$$A_{t+1} = P_t\exp(-c_{pa}A_t) + A_t(1 - \mu_a). \quad (3)$$

The quantity $b > 0$ is the average number of larvae recruited per adult per unit time in the absence of cannibalism. The fractions μ_l and μ_a are the larval and adult probabilities, respectively, of dying from causes other than cannibalism. The exponential nonlinearities account for the cannibalism of eggs by both larvae and adults and the cannibalism of pupae by adults. The fractions $\exp(-c_{ea}A_t)$ and $\exp(-c_{el}L_t)$ are the probabilities that an egg laid between times t and $t + 1$ is not eaten in the presence of A_t adults and L_t larvae. Cannibalism of larvae by adults and of pupae and callows by larvae typically occurs at much reduced rates and is assumed negligible in the model. The fraction $\exp(-c_{pa}A_t)$ is the survival probability of a pupa in the presence of A_t adults. The coefficients c_{ea}, c_{el}, and $c_{pa} \geq 0$ determine the strength of the cannibalism and are called the "cannibalism coefficients." It is assumed here, based on present knowledge, that the only significant source of pupal mortality is adult cannibalism.

Eqs. 1–3 define a (three dimensional) map of the larval, pupal, and adult numbers from one point of time to the next. In the remainder of this section, we try to understand as much as possible about the dynamics implied by these equations, that is to say, about the sequences of triples (L_t, P_t, A_t) generated by these equations from initial values (L_0, P_0, A_0). Any knowledge we can obtain about these "orbits" will tell us something about the long-term predictions of the model equations.

To study the dynamics implied by a set of model equations like Eqs. 1–3, a standard procedure is to locate equilibrium points and to determine their local stability properties. It is perhaps not surprising that a complete analytical description of equilibrium stability in terms of the system parameters is not obtainable for this system of nonlinear difference equations. There is a simplified case, however, for which a complete analytical description of the equilibrium stability region (local asymptotic stability) can be given. Moreover, in this case a description can also be given of the dynamics resulting when equilibrium stability is lost by changes in parameters across the boundary of this region. This simplified case occurs when larval cannibalism of eggs is not present, i.e., $c_{el} = 0$. In order to gain some insight into the possible dynamics of the model (Eqs. 1–3), we give the analytical results for this special case.

Mathematical analysis: larval cannibalism of eggs is absent

Equilibria are solutions (L, P, A) of the three equations

$$L = bA \exp(-c_{ea}A), \tag{4}$$

$$P = L(1 - \mu_l), \tag{5}$$

$$A = P \exp(-c_{pa}A) + A(1 - \mu_a). \tag{6}$$

Clearly, $(L, P, A) = (0, 0, 0)$ is an equilibrium. The only other non-negative equilibrium is the positive equilibrium $(L, P, A) = (L^*, P^*, A^*)$ given by the formulae

$$A^* = (c_{ea} + c_{pa})^{-1}\ln(b(1 - \mu_l)/\mu_a), \tag{7}$$

$$L^* = bA^*\exp(-c_{ea}A^*), \tag{8}$$

$$P^* = L^*(1 - \mu_l), \tag{9}$$

when

$$b > \mu_a/(1 - \mu_l). \tag{10}$$

The local stability of an equilibrium point is determined by the eigenvalues of the Jacobian (matrix of partial derivatives with respect to each state variable) of the right-hand sides of Eqs. 1–3 evaluated at the equilibrium point (Lankshmikantham and Trigiante 1988). If these eigenvalues lie inside the unit circle of the complex plane then the equilibrium is (locally asymptotically) stable. An eigenvalue outside this unit circle implies instability of the equilibrium.

The Jacobian at the origin is easily shown to have a dominant real and positive eigenvalue that is >1 if and only if Eq. 10 holds. Thus, the extinction state (0, 0, 0) is unstable if and only if a positive equilibrium exists. If Eq. 10 does not hold, the extinction state is stable and the population disappears from any initial state.

The Jacobian at the positive equilibrium (Eqs. 7–9) is complicated to analyze. Nonetheless a complete description of the region of parameter values within which all eigenvalues lie inside the complex unit circle can be given as follows. For any μ_l in the interval [0, 1) and any "cannibalism ratio"

$$r = \frac{c_{pa}}{c_{ea}} \neq 1, \tag{11}$$

define the following functions of μ_a:

$$b_e(\mu_a) = \frac{\mu_a}{1 - \mu_l}, \tag{12}$$

$$b_2(\mu_a) = \left(\frac{\mu_a}{1 - \mu_l}\right)\exp\left(\frac{2}{\mu_a}\right), \tag{13}$$

$$b_l^{\pm}(\mu_a) = \left(\frac{\mu_a}{1 - \mu_l}\right)\exp\left(\frac{K^{\pm}(\mu_a, r)}{\mu_a}\right), \tag{14}$$

where

$$K^{\pm}(\mu_a, r) = \frac{1}{2}\left[\frac{1 + r}{1 - r}\right] \cdot\left\{-(r - 3)\mu_a - 1 \pm \sqrt{[(r - 3)\mu_a + 1]^2 + 4(1 - r)(1 - \mu_a)(2\mu_a + 1)}\right\}. \tag{15}$$

In the (μ_a, b)-plane the functions $b = b_2(\mu_a)$ and $b = b_l^{\pm}(\mu_a)$ define curves on which the Jacobian has eigenvalues on the complex unit circle. On the curve $b = b_2(\mu_a)$ the Jacobian has an eigenvalue equal to -1 and on the curve defined by $b = b_l^{\pm}(\mu_a)$ the Jacobian has a pair of complex conjugate eigenvalues lying on the unit circle. For no parameter values is $+1$ an eigenvalue. Thus, these curves define the boundaries of the stability region in the (μ_a, b)-plane. The possible configurations of these boundaries depend on the cannibalism ratio r and are shown in Fig. 1.

A bifurcation (or final state) diagram allows the long-term behavior of the LPA model to be visualized as a function of a particular parameter. A sample of the kinds of bifurcations that can occur are illustrated in Fig. 2. If the boundary of the stability region in the (μ_a, b)-plane is crossed, then the positive equilibrium (Eqs. 7–9) loses its stability. If the boundary defined

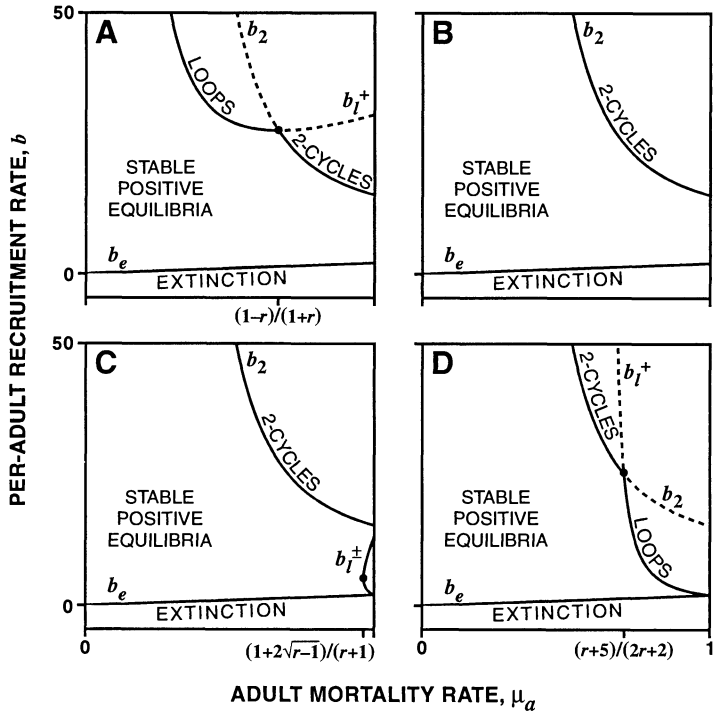

FIG. 1. The four possible configurations of the stable equilibrium and 2-cycle/invariant loop bifurcation boundaries in the $\mu_a - b$ plane for the LPA model (Eqs. 1–3) with no larval cannibalism of eggs ($c_{el} = 0$) as they depend on the ratio $r = c_{pa}/c_{ea}$ of cannibalism coefficients. (A) occurs when $0 < r < 1$ and is drawn here for $r = 0.2$. (B) occurs when $1 < r < 2$ and is drawn here for $r = 1.6$. (C) occurs when $2 < r < 3$ and is drawn here for $r = 2.9$. (D) occurs when $r > 3$ and is drawn here for $r = 9.0$. In all cases $\mu_l = 0.5128$ and the functions $b_e(\mu_a)$, $b_2(\mu_a)$, and $b_l^\pm(\mu_a)$ are defined in Eqs. (12–14).

by $b = b_2(\mu_a)$ is crossed then there is a bifurcation to a stable 2-cycle (see Fig. 2B). If the boundary defined by $b = b_l^\pm(\mu_a)$ is crossed, then there is a bifurcation to an "invariant loop" (see Fig. 2A). This means that there exists a closed loop in the (L, P, A) phase plane that is invariant under Eqs. 1–3 (i.e., orbits starting on the loop will remain on the loop). The orbits on the loop are, in general, aperiodic or "chaotic" (although "period locking" can occur). Orbits starting nearby the loop are attracted to the loop.

Numerical analysis: larval cannibalism of eggs is present

While the above analysis is for the case of no larval cannibalism ($c_{el} = 0$) we can expect similar kinds of stability regions and bifurcation scenarios in the (μ_a, b)-plane when larval cannibalism is present ($c_{el} > 0$). A numerically calculated stability region is shown in Fig. 3 for this case using parameter values estimated for a laboratory population (see Table 1). As before, the positive equilibrium destabilization boundaries are of two types. There is a boundary at which a bifurcation to a branch of 2-cycle solutions occurs, and there is a boundary at which bifurcation to an invariant loop occurs. As one of these boundaries is crossed a "stable" bifurcation usually occurs, that is to say, the resulting branch of bifurcating 2-cycles or invariant loops exists outside of the stability region, and the 2-cycles and loops are "locally stable" or "locally attracting." However, numerical evidence indicates that in our model an "unstable" bifurcation of 2-cycles can occur, in which case the 2-cycles exist locally just inside the stability region near the boundary and are unstable. This seems to occur along the rising portion of the 2-cycle bifurcation boundary (see Fig. 3). The bifurcating branch "turns around," however, and stabilizes before returning to the region of instability (i.e., a saddle-node bifurcation occurs). This creates the interesting possibility of multiple attractors in our model (and hysteresis effects). For parameter values just inside the region of stability, but near the rising portion of the 2-cycle bifurcation boundary, there exists both a stable equilibrium and a stable 2-cycle.

Three bifurcation diagrams associated with the stability diagram in Fig. 3 are shown in Fig. 4. With $b = 5$ (Fig. 4A) there are stable positive equilibria until at very high levels of adult mortality the boundary of the stability region is crossed, which leads to an invariant loop. An increase in the birth rate to the experimentally determined value of $b = 11.68$ (see Table 1) alters the system's behavior (Fig. 4B). At very low values of mortality there are stable positive equilibria, but as adult mortality is increased stable equilibria bifurcate to stable 2-cycles. Still higher rates of mortality yield a very small region of multiple attractors ($0.357 \leq \mu_a \leq 0.363$) where stable equilibria coexist with stable 2-cycles. As μ_a increases, the stable positive equilibria persist while the stable 2-cycles disappear. At high values of adult mortality there is a bifurcation to an invariant loop. In the third example, with $b = 20$ (Fig. 4C), there are stable 2-cycles until $\mu_a = 0.628$. For $0.628 \leq \mu_a \leq 0.723$ there occur multiple attractors: initially stable 2-cycles together with stable fixed points followed by 2-cycles co-occurring with invariant

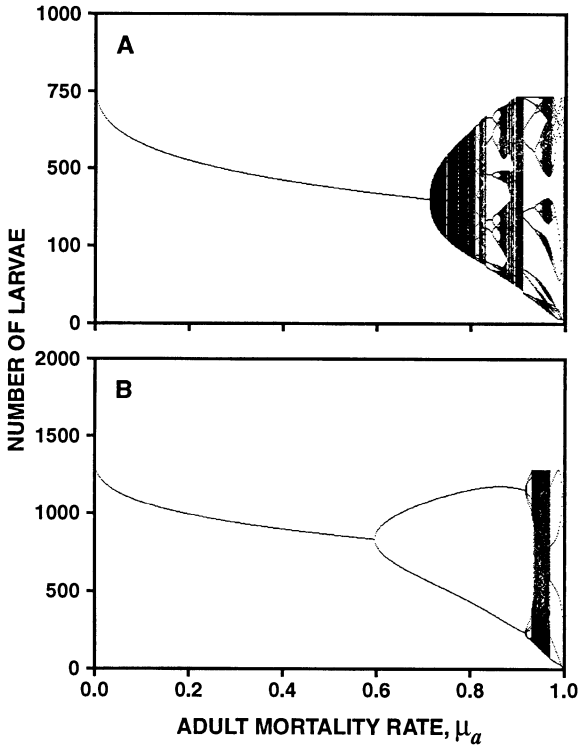

FIG. 2. Bifurcation diagrams for the LPA model (Eqs. 1–3), with no larval cannibalism of eggs, using adult mortality, μ_a, as the bifurcation parameter. In these examples $r = 9$ (case D in Fig. 1). In example (A) we set $b = 20$. As μ_a increases there is a bifurcation from a stable fixed point attractor to an invariant loop as the boundary defined by $b = b_1^{\pm}(\mu_a)$ is crossed. In example (B) we set $b = 35$. As μ_a increases there is a bifurcation to a 2-cycle as the boundary defined by $b = b_2(\mu_a)$ is crossed.

loops. These multiple attractors are explained by a "subcritical bifurcation" of 2-cycles from the equilibrium at the point $\mu_a = 0.628$, which gives rise to a branch of unstable 2-cycles for $\mu_a > 0.628$. This branch "turns around" at $\mu_a = 0.723$ where a saddle-node bifurcation occurs, giving rise to large-amplitude 2-cycles for $\mu_a < 0.723$ (Fig. 4). For $\mu_a > 0.723$ the dynamics are quite complex.

The LPA model (Eqs. 1–3) incorporates a characteristic time scale, namely, that larvae at time t become pupae at time $t + 1$, which, in turn, emerge as new adults at time $t + 2$. This time scale is experimentally testable and can be visualized in the simulated time series (Fig. 5). In the case of the 2-cycle there are two typical sequences: high numbers of larvae ($L_t = 325$), pupae ($P_{t+1} = 158$), and new adults ($A_{t+2} = 118$) and low numbers of larvae ($L_t = 18$), pupae ($P_{t+1} = 9$), and new adults ($A_{t+2} = 106$). In the case of a stable point attractor, the time scale combines with the stage interactions to yield constant animal numbers (Fig. 5). While more complex, aperiodic cycles are still bound by the basic biology of the beetle. Larval numbers at time t in this case are still followed by a corresponding group of pupae at time $t + 1$ and so on; the stage interactions on the characteristic time scale produce the irregular, unpredictable behavior of aperiodicity or "chaos" (Fig. 5).

There is an important final point to be made about the stable equilibria of our model Eqs. 1–3. "Almost all" orbits that approach a stable equilibrium do so in an oscillatory manner. This is proved analytically by showing that the cubic polynomial characteristic equation for the eigenvalues of the Jacobian obtained from Eqs. 1–3 by linearization at a stable equilibrium can never have three positive real roots between 0 and 1. Thus, there is always at least one negative real eigenvalue between -1 and 0 or a pair of complex conjugate eigenvalues of magnitude <1. In either case this fact implies that orbits near the equilibrium have either a "period two" damped oscillation or an aperiodic damped oscillation (except for at most a two-dimensional manifold of orbits embedded in three-dimensional phase space). Thus, in the stable equilibrium regions of Figs. 1 and 3 orbits will generally exhibit transitory damped oscillations in their approach to the equilibrium. While these damped oscillations will be mild for parameter values near the lower boundary of the stability region, adjoining the extinction region, they will be pronounced for parameter values near the 2-cycle and the invariant loop bifurcation boundaries. It follows that transient behavior might make sustained oscillations indistinguishable from slowly damped equilibration for orbits viewed over finite lengths of time. Consequently, the bifurcation boundaries, which are theoretically sharply defined, become blurred from a practical point of view.

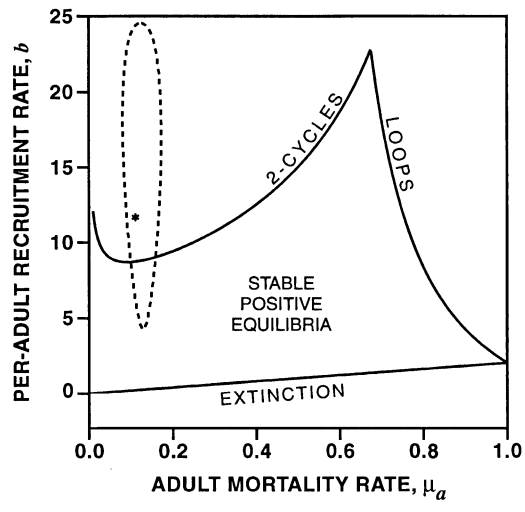

FIG. 3. Stability boundaries for the LPA model (Eqs. 1–3) for parameter values based on the experimental data (Table 1, all). The asterisk locates the estimated values of $b = 11.68$ and $\mu_a = 0.1108$. The elongated closed curve (– – –) represents a 95% joint confidence region for b and μ_a based on the profile likelihood.

TABLE 1. Maximum likelihood (ML) and conditional least squares (CLS) parameter estimates for the three-state-variable *Tribolium* model.

Parameter	Replicate A		B		C		D		All*	
	ML	CLS	ML	CLS	ML	CLS	ML	CLS	ML	95% CI
b	19.8495	23.3688	15.4928	11.2483	5.5380	5.3422	9.1323	7.2024	11.6772	(6.2, 22.2)
μ_a	0.0959	0.0934	0.1002	0.0930	0.1477	0.1468	0.1034	0.1099	0.1108	(0.07, 0.15)
μ_l	0.4725	0.4726	0.5009	0.5014	0.5082	0.5082	0.5647	0.5646	0.5129	(0.43, 0.58)
c_{ea}	0.0157	0.0175	0.0127	0.0087	0.0059	0.0044	0.0094	0.0068	0.0110	(0.0040, 0.0180)
c_{el}	0.0100	0.0098	0.0100	0.0105	0.0073	0.0080	0.0079	0.0080	0.0093	(0.0081, 0.0105)
c_{pa}	0.0195	0.0198	0.0168	0.0174	0.0179	0.0180	0.0168	0.0162	0.0178	(0.0154, 0.0207)

* The 95% confidence intervals (CI) were calculated from profile likelihoods. The ML estimates of the variances and covariances (matrix $\hat{\boldsymbol{\Sigma}}$) of the random elements are $\hat{\sigma}_{11} = 0.2771$, $\hat{\sigma}_{12} = 0.02792$, $\hat{\sigma}_{13} = 0.009796$, $\hat{\sigma}_{22} = 0.4284$, $\hat{\sigma}_{23} = -0.008150$ and $\hat{\sigma}_{33} = 0.01112$.

STATISTICAL METHODS

Stochastic model

In this section, we describe our approach to connecting the LPA model with time series data. The approach can be used in conjunction with many other difference equation models of population dynamics, and so we treat the topic in some detail. Interested readers should also consult Ludwig and Walters (1989), Hilborn and Walters (1992), and Carpenter et al. (1994) for alternative approaches, particularly for situations involving observation errors.

In order to conduct any statistical inferences, the deterministic difference equations must be converted to stochastic difference equations. The model must include a probabilistic portion that specifies how the variability in the data arose. For the LPA model (Eqs. 1–3), adding noise on a logarithmic scale produces the following stochastic model:

$$L_{t+1} = bA_t\exp(-c_{ea}A_t - c_{el}L_t + E_{1t}), \tag{16}$$

$$P_{t+1} = L_t(1 - \mu_l)\exp(E_{2t}), \tag{17}$$

$$A_{t+1} = [P_t\exp(-c_{pa}A_t) + A_t(1 - \mu_a)]\exp(E_{3t}). \tag{18}$$

Here $[E_{1t}, E_{2t}, E_{3t}]' = \boldsymbol{E}_t$ is a random vector and is assumed to have a trivariate normal distribution with a mean vector of $\mathbf{0}$ and a variance-covariance matrix of $\boldsymbol{\Sigma}$. Covariances among E_{1t}, E_{2t}, and E_{3t} at any given time t are assumed (and represented by off-diagonal elements of $\boldsymbol{\Sigma}$), but we expect the covariances between times to be small by comparison. Thus we assume that $\boldsymbol{E}_0, \boldsymbol{E}_1, \ldots$ are uncorrelated.

The stochastic construction represented by Eqs. 16–18 has a number of statistical advantages. First, on a logarithmic scale the model is of the general form

$$\boldsymbol{W}_{t+1} = \boldsymbol{h}(\boldsymbol{W}_t) + \boldsymbol{E}_t, \tag{19}$$

where $\boldsymbol{W}_t = [\ln L_t, \ln P_t, \ln A_t]'$ is the column vector of log-transformed state variables, $\boldsymbol{h}(\boldsymbol{W}_t) = [\ln\{bA_t\exp(-c_{ea}A_t - c_{el}L_t)\}, \ln\{(1 - \mu_l)L_t\}, \ln\{P_t\exp(-c_{pa}A_t) + (1 - \mu_a)A_t\}]'$ is a column vector of functions, and $\boldsymbol{E}_t$ has a multivariate normal $(\mathbf{0}, \boldsymbol{\Sigma})$ distribution. A stochastic model of this form is a type of multivariate, nonlinear, autoregressive model. Development of statistical methods for nonlinear autoregressive models (estimation, testing, evaluation) has received much attention in recent years (Tong 1990). Second, the nonlinear map of the deterministic model on the logarithmic scale is preserved in the conditional expected values of $\ln L_{t+1}$, $\ln P_{t+1}$, $\ln A_{t+1}$ given values of L_t, P_t, and A_t:

$$\mathrm{E}(\ln L_{t+1} \mid L_t = l_t, P_t = p_t, A_t = a_t) = \ln[ba_t\exp(-c_{ea}a_t - c_{el}l_t)], \tag{20}$$

$$\mathrm{E}(\ln P_{t+1} \mid L_t = l_t, P_t = p_t, A_t = a_t) = \ln[(1 - \mu_l)l_t], \tag{21}$$

$$\mathrm{E}(\ln A_{t+1} \mid L_t = l_t, P_t = p_t, A_t = a_t) = \ln[p_t\exp(-c_{pa}a_t) + (1 - \mu_a)a_t]. \tag{22}$$

Thus the stochastic version retains the essential dynamical properties that we described in the *Mathematical models* section. Other statistical advantages are that the model is easy to simulate and that parameter estimates are straightforward to compute from data.

The stochastic construction has biological advantages as well. First, the noise structure is realistic. Ecologists have drawn a distinction between demographic (intrinsic chance variation among individuals in the timing of births and deaths) and environmental (chance variation from extrinsic sources affecting many individuals) fluctuations in populations (see May 1974*b*, Shaffer 1981, Simberloff 1988). Models with noise additive on a logarithmic scale correspond to environmental-type fluctuations (Dennis et al. 1991). At the large sizes typical of *Tribolium* cultures, we expect the variability component due to environmental fluctuations to outweigh the component due to demographic fluctuations (Dennis and Costantino 1988). Second, the model allows for covariance of fluctuations in larvae, pupae, and adults in a given time period, as described by the covariance of the elements in $\boldsymbol{E}_t$. A bad/good week for adults is likely related to having a bad/good week for larvae, etc. Autocovariances of the noise el-

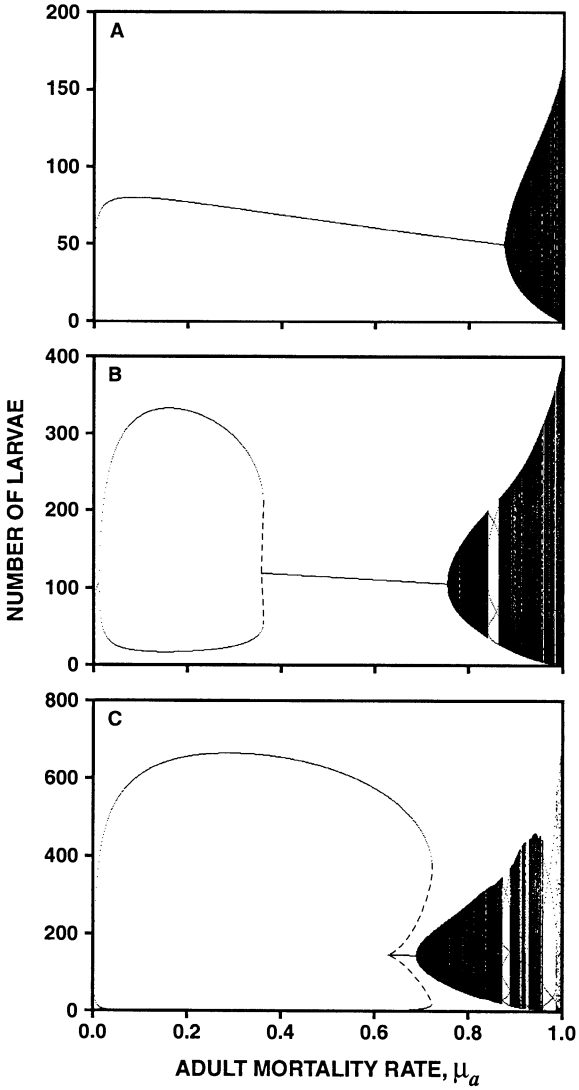

FIG. 4. Bifurcation diagrams for the LPA model (Eqs. 1–3) for parameter values based on the experimental data (Table 1, all, and Fig. 3). In case (A) we set $b = 5$. As μ_a increases there is a bifurcation from a stable fixed-point attractor to an invariant loop as the stability boundary is crossed at $\mu_a = 0.876$. Case (B) represents the estimated value of $b = 11.68$. There is a bifurcation to a 2-cycle at a small value of $\mu_a = 0.011$. As adult mortality increases, the population reenters the region of parameter space where the positive equilibria are stable (see Fig. 3). However, there is a narrow interval $0.357 < \mu_a < 0.363$ where a stable 2-cycle and fixed-point equilibria coexist, separated by an unstable 2-cycle (– – –). In case (C) we set $b = 20$. In this case, when the population reenters the region of stable equilibria (at $\mu_a = 0.628$) a branch of unstable 2-cycles bifurcates to the right (– – –). This branch "turns around" at $\mu_a = 0.723$ where a saddle-node bifurcation occurs, creating the stable large-amplitude 2-cycles shown in (C). In the meantime, prior to $\mu_a = 0.628$ the population crosses the equilibrium stability boundary at $\mu_a = 0.689$ where stable invariant loops bifurcate from the equilibria. This complicated scenario creates a region $0.628 < \mu_a < 0.723$ of multiple attractors. Specifically, there coexists stable equilibria and stable 2-cycles for $0.628 < \mu_a < 0.689$ and stable invariant loops and stable 2-cycles for $0.689 < \mu_a < 0.723$. For larger values of b the dynamics are even more complex.

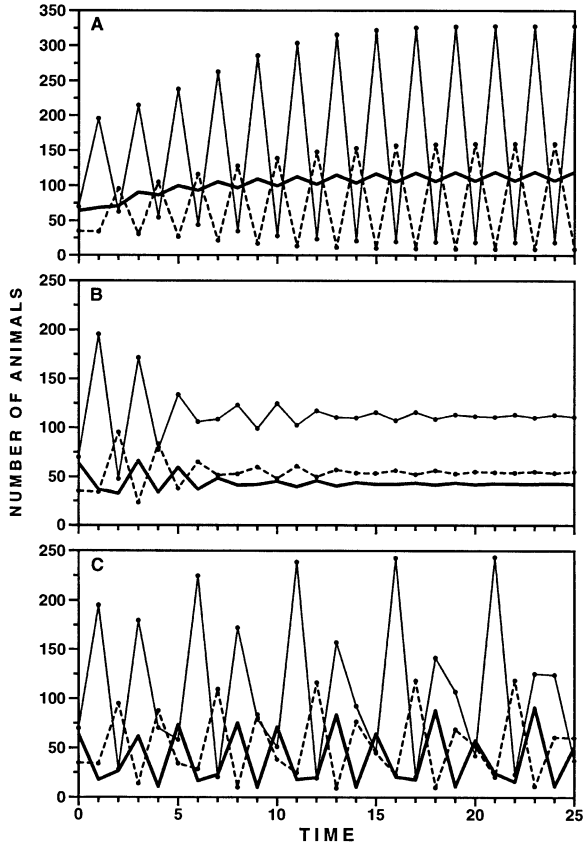

FIG. 5. Simulated time series corresponding to the three classes of behavior indicated in Figs. 3 and 4. Parameters are based on the experimental data (Table 1, all). Case (A) represents the estimated value of $\mu_a = 0.1108$, which produces a stable 2-cycle. In case (B) we set $\mu_a = 0.6$, which results in a stable equilibrium. In case (C) we set $\mu_a = 0.9$, which yields an aperiodic cycle.

ements through time, though, are not expected to be important compared to the covariances between the elements within a time, provided the underlying dynamics (deterministic equations) are specified correctly. Finally, the different scales of variability for larvae, pupae, and adults are accounted for through the parameters on the main diagonal of the variance-covariance matrix Σ.

Likelihood function

The stochastic LPA model (Eqs. 16–18) provides an explicit likelihood function. A likelihood function gives the chance that an outcome of a proposed stochastic mechanism would result in the observed data, relative to all other possible outcomes. A likelihood function is a fundamental tool in statistical inference (see Stuart and Ord 1991) and represents the crucial connection between model and data. Data for a particular *Tribolium* population are a realization of the joint stochastic variables L_t, P_t, and A_t. The data take the form of a trivariate time series: (l_0, p_0, a_0), (l_1, p_1, a_1),

. . . , (l_q, p_q, a_q) (see Fig. 7). Let $\boldsymbol{w}_t$ denote the column vector of observations at time t: $\boldsymbol{w}_t = [\ln l_t, \ln p_t, \ln a_t]'$. Suppose θ denotes the unknown parameters in the functions in $\boldsymbol{h}(\cdot)$ of Eq. 19 (that is, the parameters in the deterministic model equations). Additional unknown parameters are in the variance-covariance matrix, $\boldsymbol{\Sigma}$. The likelihood function, $L(\boldsymbol{\theta}, \boldsymbol{\Sigma})$, is given by

$$L(\boldsymbol{\theta}, \boldsymbol{\Sigma}) = \prod_{t=1}^{q} p(\boldsymbol{w}_t | \boldsymbol{w}_{t-1}), \tag{23}$$

where $p(\boldsymbol{w}_t | \boldsymbol{w}_{t-1})$ is the joint transition probability density function (pdf), that is, the joint pdf for $\boldsymbol{W}_t$ conditional on $\boldsymbol{W}_{t-1} = \boldsymbol{w}_{t-1}$ and evaluated at $\boldsymbol{w}_t$. It is a multivariate normal pdf with a mean vector of $\boldsymbol{h}(\boldsymbol{w}_{t-1})$ and a variance-covariance matrix of $\boldsymbol{\Sigma}$:

$$p(\boldsymbol{w}_t | \boldsymbol{w}_{t-1}) = |\boldsymbol{\Sigma}|^{-1/2}(2\pi)^{-3/2} \cdot \exp[-(\boldsymbol{w}_t - \boldsymbol{h}_{t-1})'\boldsymbol{\Sigma}^{-1}(\boldsymbol{w}_t - \boldsymbol{h}_{t-1})/2], \tag{24}$$

where $\boldsymbol{h}_{t-1}$ denotes $\boldsymbol{h}(\boldsymbol{w}_{t-1})$. Most of the actual statistical calculations utilize the log-likelihood given by

$$\begin{aligned} \ln L(\boldsymbol{\theta}, \boldsymbol{\Sigma}) &= \sum_{t=1}^{q} \ln p(\boldsymbol{w}_t | \boldsymbol{w}_{t-1}) \\ &= -q(3/2)\ln(2\pi) - (q/2)\ln|\boldsymbol{\Sigma}| \\ &\quad - (1/2)\sum_{t=1}^{q} (\boldsymbol{w}_t - \boldsymbol{h}_{t-1})'\boldsymbol{\Sigma}^{-1}(\boldsymbol{w}_t - \boldsymbol{h}_{t-1}). \end{aligned} \tag{25}$$

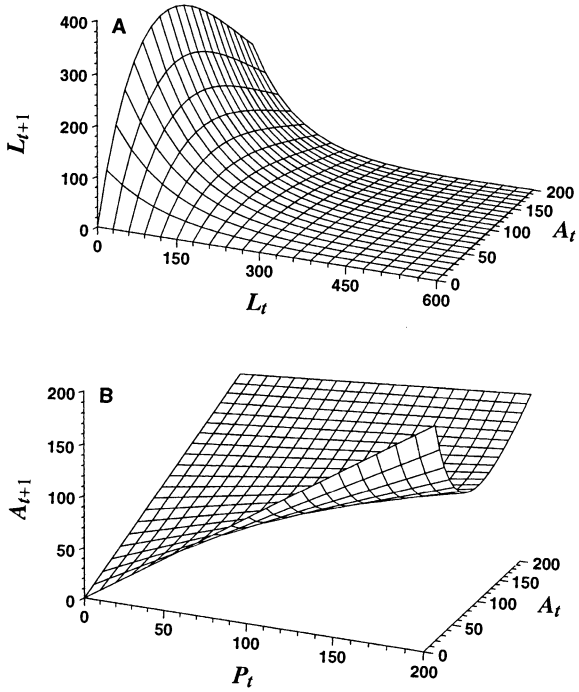

FIG. 6. Response surfaces in the LPA model (Eqs. 1–3). Plot (A) shows how larval numbers at time $t + 1$ are a function of the number of larvae and adults at time t. Plot (B) shows how adult numbers at time $t + 1$ are a function of the number of pupae and adults at time t. On a logarithmic scale, these surfaces represent predicted values for one-step transitions.

Maximum likelihood estimates

Maximum likelihood (ML) estimates of parameters in $\boldsymbol{\theta}$ and $\boldsymbol{\Sigma}$ are those values that jointly maximize $L(\boldsymbol{\theta}, \boldsymbol{\Sigma})$, or $\ln L(\boldsymbol{\theta}, \boldsymbol{\Sigma})$. No closed formulas for such estimates exist, although it can be shown that the ML estimates of the parameters in $\boldsymbol{\Sigma}$ can be written in terms of the ML estimates of parameters in $\boldsymbol{\theta}$ (see paragraph containing Eq. 34 for formula). The ML estimates of parameters in $\boldsymbol{\theta}$ must be obtained numerically for any particular data set. We have found that maximizing the log-likelihood using the Nelder-Mead simplex algorithm (see Olsson and Nelson 1975, Press et al. 1986) is convenient, reliable, and easy to program. The algorithm only requires a subroutine to evaluate the log-likelihood (Eq. 25) for any particular set of parameter values.

ML estimates for the stochastic LPA model (Eqs. 16–18) have desirable statistical properties. ML estimates are asymptotically unbiased (bias approaches zero as sample size increases), asymptotically efficient (variance approaches theoretical lowest bound as sample size increases), and asymptotically normally distributed (allowing construction of approximate confidence intervals) (see Stuart and Ord 1991). For nonlinear time series models, the sample size is the number of observations in the time series, and the theorems about ML properties generally require that the stochastic model have a statistical equilibrium in the form of a stationary distribution (Tong 1990). A nonlinear autoregressive model of the form of Eq. 19 will typically have a stationary distribution when every trajectory of the underlying deterministic model $\boldsymbol{w}_{t+1} = \boldsymbol{h}(\boldsymbol{w}_t)$ has a bounded attractor. It is easy to demonstrate with simulations that the stochastic LPA model possesses a stationary distribution (see *Discussion* section, Fig. 22).

However, the properties of ML estimates do not hold if the model is a poor description of the underlying stochastic mechanisms producing the data. In particular, if the noise vector $\boldsymbol{E}_t$ in Eq. 19 does not have a multivariate normal distribution, or is correlated through time, then the ML estimates could be biased. Since we aim to identify dynamic behavior by estimating where the parameters in $\boldsymbol{\theta}$ are in parameter space (Fig. 3), an alternative estimation method that yields more robust parameter estimates is useful.

Conditional least squares estimates

Conditional least squares (CLS) estimates relax most distributional assumptions about $\boldsymbol{E}_t$ (Klimko and Nelson 1978, Tong 1990). As such, we use CLS estimates as a check on the ML estimates. If the normality assumptions are reasonable, both ML and CLS estimates are consistent (converge to the true parameters as sam-

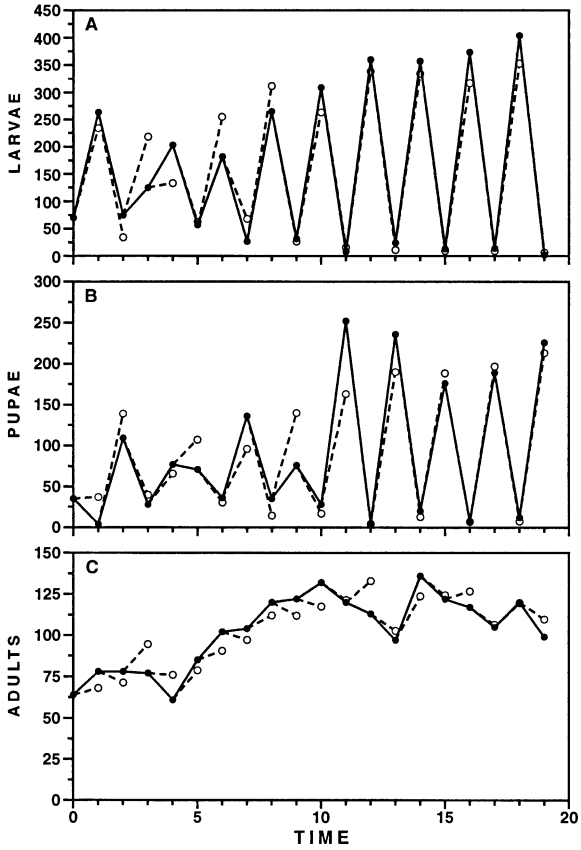

FIG. 7. Time series data (●) and one-step forecasts (○) for control replicate A of Desharnais and Liu (1987). Solid lines connect the observed census data. Dashed lines connect the observed numbers at time t with the forecast at time $t + 1$.

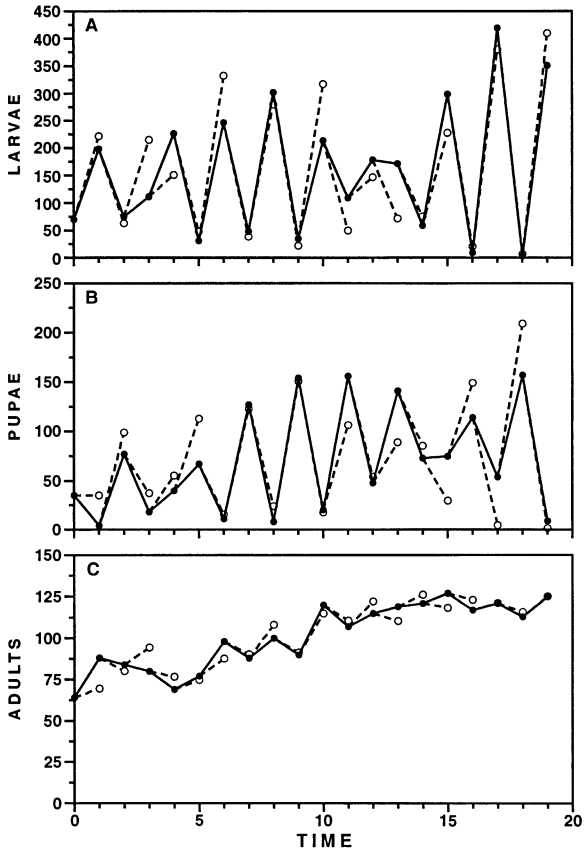

FIG. 8. Time series data (●) and one-step forecasts (○) for control replicate B of Desharnais and Liu (1987). Solid lines connect the observed census data. Dashed lines connect the observed numbers at time t with the forecast at time $t + 1$.

ple size increases) and thus should be similar. CLS estimates remain consistent, though, even if $\boldsymbol{E}_t$ is non-normal and autocorrelated, provided the stochastic model has a stationary distribution (Klimko and Nelson 1978, Tong 1990).

CLS estimates for multivariate time series models have not received much study; the estimates are typically described only for univariate models (Tong 1990). Fortunately, in the LPA model, CLS estimates reduce to 3 univariate cases, because any given parameter (e.g., μ_l) does not appear in more than one model equation (Eq. 17). CLS estimates are based on the sum of squared differences between the value of a variable observed at time t and its expected (or one-step forecast) value, given the observed state of the system at time $t - 1$. For the LPA model, there are three such conditional sums of squares:

$$Q_1(\boldsymbol{\theta}_1) = \sum_{t=1}^{q} \{\ln l_t - \ln[b a_{t-1} \exp(-c_{ea} a_{t-1} - c_{el} l_{t-1})]\}^2, \quad (26)$$

$$Q_2(\boldsymbol{\theta}_2) = \sum_{t=1}^{q} \{\ln p_t - \ln[(1 - \mu_l) l_{t-1}]\}^2, \quad (27)$$

$$Q_3(\boldsymbol{\theta}_3) = \sum_{t=1}^{q} \{\ln a_t - \ln[p_{t-1} \exp(-c_{pa} a_{t-1}) + (1 - \mu_a) a_{t-1}]\}^2. \quad (28)$$

Here $\boldsymbol{\theta}_1 = [b, c_{el}, c_{ea}]'$, $\boldsymbol{\theta}_2 = \mu_l$, and $\boldsymbol{\theta}_3 = [c_{pa}, \mu_a]'$ are the parameter vectors from the individual model equations (Eqs. 16–18). The conditional sums of squares are constructed on the logarithmic scale because that is the scale on which we assume noise is additive (Eq. 19). The conditional one-step expected values appearing in Eqs. 26–28 are from Eqs. 20–22.

CLS estimates minimize the conditional sums of squares (Eqs. 26–28). Three separate numerical minimizations are required, one for each of the sums of squares. We find the Nelder-Mead simplex algorithm convenient. Alternatively, the CLS estimates can be obtained by minimizing Q_1, Q_2, and Q_3 in turn with a standard nonlinear regression package. The estimates of the parameters in the variance-covariance matrix of

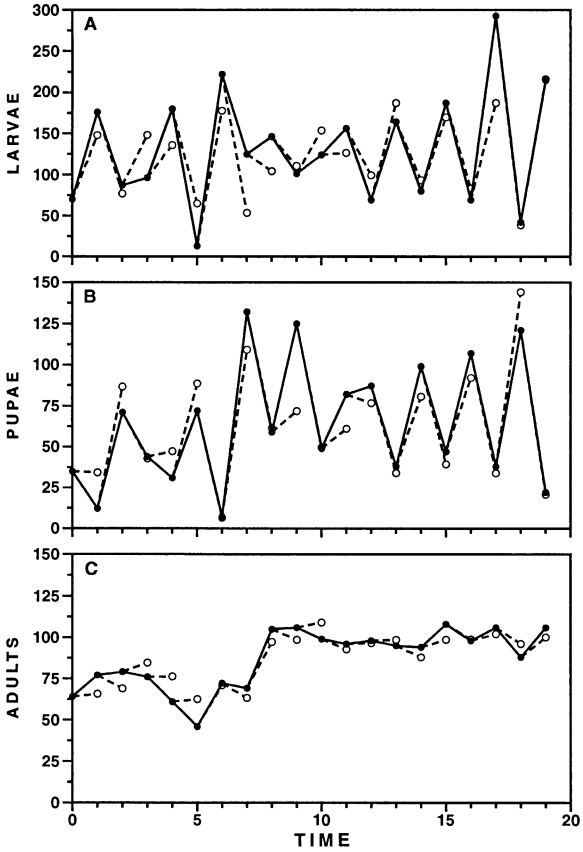

FIG. 9. Time series data (●) and one-step forecasts (○) for control replicate C of Desharnais and Liu (1987). Solid lines connect the observed census data. Dashed lines connect the observed numbers at time t with the forecast at time $t + 1$.

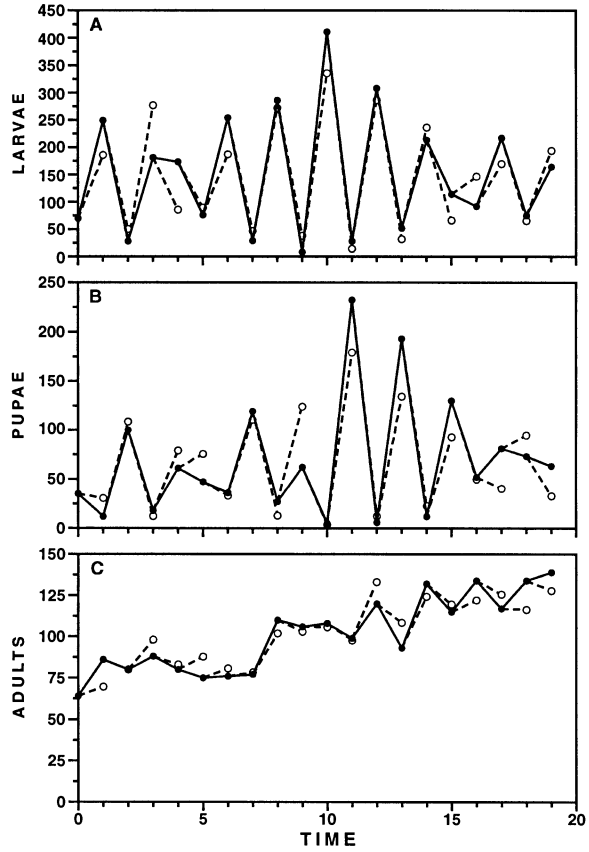

FIG. 10. Time series data (●) and one-step forecasts (○) for control replicate D of Desharnais and Liu (1987). Solid lines connect the observed census data. Dashed lines connect the observed numbers at time t with the forecast at time $t + 1$.

$\boldsymbol{E}_t$ are then found from the sums of squares and cross products matrix constructed using the conditional residuals (observed log-scale variable at time t minus estimated expected value given variables at time $t - 1$).

Hypothesis testing and confidence intervals

One test of a dynamic model is that we would expect replicate populations to have the same parameter values. Laboratory *Tribolium* populations come as close as is practical in population biology to being replicates, provided careful laboratory protocol is followed. Under such circumstances, we can test whether or not the parameter estimates obtained by fitting the model separately to the replicates could have arisen from one common model with identical parameters.

The test is a likelihood ratio test (Stuart and Ord 1991). Suppose r replicate populations are cultured and censused. The result would be r multivariate time series. It is not necessary that each culture be followed for the same total length of time. The log-likelihood for the j^{th} replicate, denoted $\ln L_j(\boldsymbol{\theta}_j, \boldsymbol{\Sigma}_j)$, is given by Eq. 25, except with q_j, $\boldsymbol{w}_{jt}$, and $\boldsymbol{h}_{j(t-1)}$ substituted for q, $\boldsymbol{w}_t$, and $\boldsymbol{h}_{t-1}$. Here q_j is the sample size for replicate j, $\boldsymbol{w}_{jt}$ is the vector of observed logarithmic population sizes for the j^{th} replicate at time t, and $\boldsymbol{h}_{j(t-1)}$ is the vector of conditional expected values for $\boldsymbol{W}_{jt}$ given $\boldsymbol{W}_{j(t-1)} = \boldsymbol{w}_{j(t-1)}$ (Eqs. 20–22). The joint log-likelihood for all r replicates, provided they are independent replicates, is the sum of the individual log-likelihoods:

$$\ln L(\boldsymbol{\theta}_1, \ldots, \boldsymbol{\theta}_r; \boldsymbol{\Sigma}_1, \ldots, \boldsymbol{\Sigma}_r) = \sum_{j=1}^{r} \ln L_j(\boldsymbol{\theta}_j, \boldsymbol{\Sigma}_j). \quad (29)$$

Here $\boldsymbol{\theta}_j$ and $\boldsymbol{\Sigma}_j$ contain the parameters for the j^{th} replicate.

The null hypothesis of the test is that the r replicates are trajectories from the stochastic model (Eqs. 19) with identical parameters:

$$H_0: \boldsymbol{\theta}_1 = \boldsymbol{\theta}_2 = \ldots = \boldsymbol{\theta}_r = \boldsymbol{\theta},$$
$$\boldsymbol{\Sigma}_1 = \boldsymbol{\Sigma}_2 = \ldots = \boldsymbol{\Sigma}_r = \boldsymbol{\Sigma}. \quad (30)$$

The alternative hypothesis is that one or more parameters among the replicates is different.

The test requires ML parameter estimates under both null and alternative hypotheses. For the alternative hypothesis, the model is fitted individually to each rep-

TABLE 2. Residual analyses. First ($\hat{\rho}_1$) and second-order ($\hat{\rho}_2$) sample autocorrelations and Lin-Mudholkar (z) test statistic for normality.

Test statistic	Replicate											
	A			B			C			D		
	Larvae	Pupae	Adults	Larvae	Pupae	Adults	Larvae	Pupae	Adults	Larvae	Pupae	Adults
$\hat{\rho}_1$	−0.04	0.05	0.30	−0.29	−0.07	0.05	0.00	0.18	0.34	−0.20	−0.38	0.03
$\hat{\rho}_2$	−0.12	0.15	−0.45	0.54*	0.56	−0.48*	−0.16	0.16	−0.17	0.06	0.13	0.08
z	1.88	2.70**	1.85	0.81	−0.85	−1.21	1.68	2.20**	2.08**	0.32	0.70	−0.63

* Significant (0.05 level of probability) j^{th} order autocorrelation if $|\hat{\rho}_j|$ exceeds 0.46.
** Significant (0.05 level of probability) departure from normality if $|z|$ exceeds 1.96.

licate (that is, Eq. 25 is maximized), to obtain the ML estimates $\hat{\boldsymbol{\theta}}_1, \ldots, \hat{\boldsymbol{\theta}}_r, \hat{\boldsymbol{\Sigma}}_1, \ldots, \hat{\boldsymbol{\Sigma}}_r$. A substitution of the ML estimates into Eq. 29 produces the maximized log-likelihood under the alternative hypothesis:

$$\ln \hat{L}_A = \ln L(\hat{\boldsymbol{\theta}}_1, \ldots, \hat{\boldsymbol{\theta}}_r; \hat{\boldsymbol{\Sigma}}_1, \ldots, \hat{\boldsymbol{\Sigma}}_r). \quad (31)$$

For the null hypothesis, we substitute $\boldsymbol{\theta}$ for $\boldsymbol{\theta}_1$, $\boldsymbol{\theta}_2$, ... and $\boldsymbol{\theta}_r$, and $\boldsymbol{\Sigma}$ for $\boldsymbol{\Sigma}_1$, $\boldsymbol{\Sigma}_2$, ... and $\boldsymbol{\Sigma}_r$ in the log-likelihood (Eq. 29). Then, ML estimates $\hat{\boldsymbol{\theta}}$ and $\hat{\boldsymbol{\Sigma}}$ are found by maximizing Eq. 29. The maximized log-likelihood under the null hypothesis then becomes

$$\ln \hat{L}_N = \ln L(\hat{\boldsymbol{\theta}}, \ldots, \hat{\boldsymbol{\theta}}; \hat{\boldsymbol{\Sigma}}, \ldots, \hat{\boldsymbol{\Sigma}}). \quad (32)$$

If the null hypothesis is true, the likelihood ratio test statistic given by

$$G^2 = -2(\ln \hat{L}_N - \ln \hat{L}_A) \quad (33)$$

will have an approximate chi-square distribution with $12(r - 1)$ degrees of freedom (the number of parameters estimated under the alternative hypothesis minus the number of parameters estimated under the null hypothesis). The conditions for the chi-square approximation to hold are the same as the conditions for asymptotic efficiency of the ML estimates: stationary distribution, large sample size, and appropriateness of the model itself.

One of the main objectives of our analyses is to classify the dynamical behavior of the system. We do this by locating the ML estimate of $\boldsymbol{\theta}$ in parameter space and identifying the type of behavior (stable point equilibrium, 2-cycles, and so on) displayed by the deterministic LPA model (Eqs. 1–3) at those parameter values. Naturally, there is uncertainty attached to the parameter estimates. However, confidence intervals for individual parameters, and joint confidence regions for sets of parameters, are straightforward to compute with likelihood methods.

We use confidence intervals and regions based on the profile likelihood. Profile likelihood intervals require much computing, but can be applied to many different types of statistical models (see McCullagh and Nelder 1989: 254, Venzon and Moolgavkar 1988). Profile likelihood intervals are only approximate, that is, their coverage frequencies asymptotically converge to 95% as the sample size (time series length) becomes large. The intervals are usually asymmetric, and typically have better small-sample coverage frequencies than do symmetric confidence intervals arising from the matrix of second derivatives of the log-likelihood function.

The profile likelihood intervals and regions are obtained by inverting a likelihood ratio test. Suppose $\boldsymbol{\beta}$ is a parameter (or vector of parameters) of interest in the vector $\boldsymbol{\theta}$, and suppose $\boldsymbol{\psi}$ is the vector of all the other parameters: $\boldsymbol{\theta} = [\boldsymbol{\beta}, \boldsymbol{\psi}]'$. We write the likelihood function as $L(\boldsymbol{\theta}, \boldsymbol{\Sigma}) = L(\boldsymbol{\beta}, \boldsymbol{\psi}, \boldsymbol{\Sigma})$. Let $\hat{\boldsymbol{\psi}}_\beta$ and $\hat{\boldsymbol{\Sigma}}_\beta$ denote the values of $\boldsymbol{\psi}$ and $\boldsymbol{\Sigma}$ formed by maximizing the likelihood for a fixed value of $\boldsymbol{\beta}$. Then $L(\boldsymbol{\beta}, \hat{\boldsymbol{\psi}}_\beta, \hat{\boldsymbol{\Sigma}}_\beta)$ taken as a function of $\boldsymbol{\beta}$ is the "profile likelihood"; evaluating this function requires a separate maximization for each value of $\boldsymbol{\beta}$. The 95% profile likelihood interval (or region) is the set of all values of $\boldsymbol{\beta}$ for which $-2[\ln L(\boldsymbol{\beta}, \hat{\boldsymbol{\psi}}_\beta, \hat{\boldsymbol{\Sigma}}_\beta) - \ln L(\hat{\boldsymbol{\theta}}, \hat{\boldsymbol{\Sigma}})] \leq \chi^2_{0.05}(\eta)$, where $\chi^2_{0.05}(\eta)$ is the 95th percentile of a chi-square distribution with η degrees of freedom, and η is the number of parameters in $\boldsymbol{\beta}$ [$\chi^2_{0.05}(\eta) \approx 3.843$ if $\boldsymbol{\beta}$ represents just one parameter]. The interval is the set of all $\boldsymbol{\beta}$ values for which a likelihood ratio test on $\boldsymbol{\beta}$ would not reject the null hypothesis.

Model evaluation

Model evaluation procedures center on the residuals defined as the differences of the logarithmic state variables and their one-step (estimated) expected values:

$$\boldsymbol{e}_t = \boldsymbol{w}_t - \hat{\boldsymbol{h}}(\boldsymbol{w}_{t-1}). \quad (34)$$

Here $\boldsymbol{e}_t$ is a vector of residuals for $\ln l_t$, $\ln p_t$, and $\ln a_t$ in a population at time t, and $\hat{\boldsymbol{h}}$ denotes the functions in $\boldsymbol{h}$ (Eqs. 20–22) evaluated at the ML parameter estimates. The ML estimate of the matrix $\boldsymbol{\Sigma}$, incidently, can be written in terms of the residuals as $\hat{\boldsymbol{\Sigma}}) = \boldsymbol{RR}'/q$, where $\boldsymbol{R} = [\boldsymbol{e}_1, \boldsymbol{e}_2, \ldots, \boldsymbol{e}_q]$ is a matrix with residual vectors as columns.

If the model fits, then $\boldsymbol{e}_1, \boldsymbol{e}_2, \ldots, \boldsymbol{e}_q$ should behave approximately like uncorrelated observations from a trivariate normal distribution. Unlike the original noise vectors, the residual vectors are, in fact, correlated, and the normality is approximate, with the quality of the approximation varying among different nonlinear time series models. Thus, autocorrelation tests and normal-

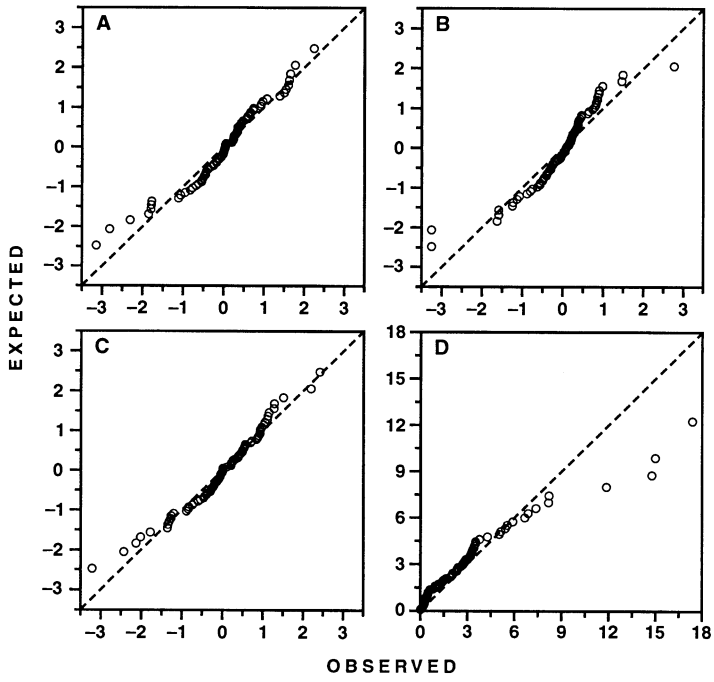

FIG. 11. Quantile-quantile (Q-Q) plots of logarithmic residuals (Eq. 34) for the LPA model fitted to the data from the four control replicates of Desharnais and Liu (1987). Parameter estimates used appear in Table 1 (all). (A) Normal Q-Q plot; larvae residuals. (B) Normal Q-Q plot; pupae residuals. (C) Normal Q-Q plot; adult residuals. (D) Chi-square Q-Q plot; multivariate residuals (quadratic forms) calculated from the residual vectors (Eq. 35).

ity tests should be used only as rough guides to potential areas in which the model is not adequate. Cox and Small (1978) provide some useful approaches to testing multivariate normality. A useful scan for outliers from multivariate normality is to calculate the quadratic form for each vector residual:

$$s_t = \boldsymbol{e}_t' \boldsymbol{\Sigma}^{-1} \boldsymbol{e}_t. \tag{35}$$

If $\boldsymbol{e}_t$ is indeed an observation from a multivariate normal $(\mathbf{0}, \boldsymbol{\Sigma})$ distribution, then s_t is an observation from a chi-square distribution with 3 df (e.g., Cox and Small 1978, Seber 1984). An estimate of $\boldsymbol{\Sigma}$, such as the ML estimate $\hat{\boldsymbol{\Sigma}}$ or the moment estimate $\tilde{\boldsymbol{\Sigma}} = \boldsymbol{RR}'/(q-1)$, must be substituted for $\boldsymbol{\Sigma}$ in Eq. 35; the chi-square distribution in practice is thus only approximate. The residuals for each individual state variable should have small autocorrelations and approximate univariate normal distributions. Tests such as the Lin-Mudholkar test for (univariate) normality against asymmetric alternatives (Lin and Mudholkar 1980, Tong 1990: 324) are useful supplements to standard normal probability plots. Standard univariate autocorrelation tests (Tong 1990: 324) are informative as well.

Failure of the model to describe some portions of the data can have two main causes. First, the distributional assumptions about the noise vector $\boldsymbol{E}_t$ in the model (Eq. 19) could be incorrect. Under such circumstances, CLS estimates are probably superior and should be used instead of ML estimates. Second, the underlying dynamics of the system, as expressed in the deterministic model (Eqs. 1–3) could be incorrectly specified. A valuable tool for studying this possibility is to plot the map and one-step transitions together using interactive three-dimensional plotting software. The underlying deterministic map (Eqs. 1–3) gives L_{t+1} as a function of L_t and A_t, P_{t+1} as a function of L_t, and A_{t+1} as a function of P_t and A_t (Fig. 6). On the logarithmic scale, these functions are essentially response surfaces representing the expected values of $\ln L_{t+1}$, $\ln P_{t+1}$, $\ln A_{t+1}$ given the values of these variables at time t. Each three-dimensional graph of surface and observations can be rotated interactively to detect areas where the surface is not adequately describing the data.

BIOLOGICAL EXPERIMENTS

Experimental protocol

We now turn our attention to the data and to the application of the procedures just described to connect the mathematical model (Eqs. 1–3) with the time series observations. First we look at the experimental protocol.

Desharnais and Costantino (1980) initiated 13 cultures of the corn oil sensitive strain of *Tribolium castaneum* Herbst with 64 young adults, 16 pupae, 20 large larvae, and 70 small larvae. Each population was contained in a half-pint milk bottle (237 ml) with 20 g of corn oil media (90% wheat flour, 5% brewer's yeast, and 5% liquid corn oil) and kept in an unlighted incubator at a temperature range of 33 ± 1°C and a relative humidity range of 56 ± 11%. Every 2 wk all stage classes, except eggs, were censused and all stage classes, including eggs, were placed in fresh media. This procedure was followed for 38 wk. After 10 wk of culture, each population was randomly assigned to one of four treatments. Three of the treatments, each with three replicates, involved demographic perturba-

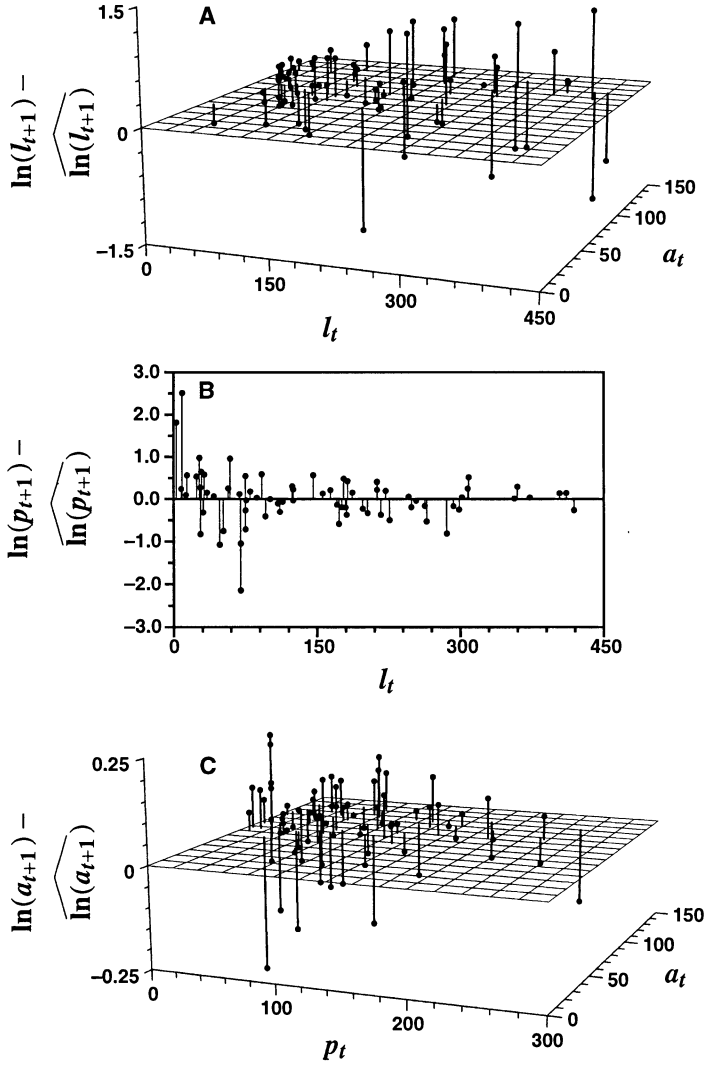

FIG. 12. Residual plots for the data from the four control replicates of Desharnais and Liu (1987). Deviations between the logarithms of the observed and predicted numbers of (A) larvae at time $t + 1$ as a function of the number of larvae and adults at time t, (B) pupae at time $t + 1$ as a function of the number of larvae at time t, and (C) adults at time $t + 1$ as a function of the number of pupae and adults at time t.

tions and one treatment, with four replicates, served as a control. The three demographic perturbations were: (1) 100 adults added, (2) all adults removed, and (3) all immatures removed. The control cultures were not disturbed. The census data are given in Table 2 of Desharnais and Liu (1987).

Parameter estimates obtained from control replicates

We fitted the stochastic model (Eqs. 16–18) to the time series of the four control replicates (see Figs. 7–10). The maximum likelihood and conditional least squares parameter estimates are given in Table 1. The CLS estimates were obtained by minimizing the conditional sums of squares (Eqs. 26–28) using the Nelder-Mead method. The ML estimates were calculated by maximizing Eq. 25 using the Nelder-Mead method. Starter values for the iterative ML calculations were CLS estimates. The ML calculations converged for other starter values as well. The ML and CLS estimates are similar, which suggests that the distributional assumptions about the noise vector $\boldsymbol{E}_t$ in Eq. 19 are reasonable.

The observed time series together with the one-step predictions, calculated from Eqs. 20–22 using the ML parameter estimates, are sketched in Figs. 7–10. Since the one-step forecasts are conditional predictions of animal numbers at time $t + 1$ given the actual numbers at time t, we attempted to incorporate that idea into the data presentation. In each figure solid lines connect the observed census data (●). Dashed lines connect the observed numbers at time t with the forecast (○) at time $t + 1$. The accuracy of a particular forecast can be judged by comparing the prediction at time $t + 1$ with that actually observed at time $t + 1$. Keep in mind that the one-step forecast, say, for the number of feeding larvae at time $t + 1$ is conditional on both the number of larvae at time t and the number of adults at time t, and not on just the number of larvae at time t. The graphs associate the data at time t with a forecast at time $t + 1$ and allow a visualization of how well

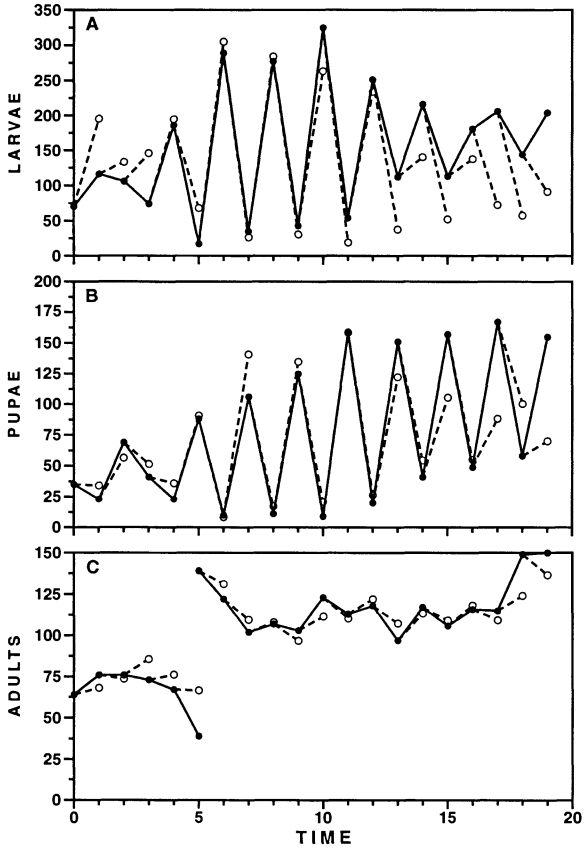

FIG. 13. Time series data (●) and one-step forecasts (○) for replicate A of Desharnais and Liu (1987) where 100 adults were added at $t = 5$. Solid lines connect the observed census data. The one-step forecasts (dashed line projections) are based on the parameter estimates obtained from the control cultures.

prediction and observation agree. In general, the graphs reveal a close association between the one-step forecasts and the actual animal counts.

Theoretically, these four populations should be arising from the same model with the same parameter values. We tested the hypothesis that the parameters are identical for all four populations (null) vs. the hypothesis that the parameter values are different between populations (alternative). We used the likelihood ratio statistic (Eq. 33) for the test. For these data, we failed to reject at the 0.05 significance level the null hypothesis that the parameters of the four control populations are identical ($G^2 = 49.6$, df = 36, $P = 0.065$).

The ML parameter estimates for the model fitted to all four control populations (Table 1, all) place the system in a zone of stable 2-cycles (asterisk, Fig. 3). The ML location of the system in parameter space is but a point estimate: how much uncertainty is attached to the estimate? Depicted in Fig. 3 is a dashed, cigar-shaped closed curve representing a 95% confidence region for the key parameters b and μ_a. The region was calculated with the profile likelihood method. The likelihood function was maximized for each point on a 100 $\times$ 100 grid of b and μ_a values. The dashed curve is a contour indicating where the likelihood ratio test statistic for two parameters equals 5.992 (the approximate 95th percentile of a chi-squared distribution with 2 df). Note that most of the confidence region lies within the zone of 2-cycles. However, the tip of the region extends into the zone of stable point equilibria, in an area where the system undergoes damped oscillations.

Distinguishing damped oscillations from sustained oscillations in a noisy environment has always been problematic. Our analysis suggests that while there are plausible values of b and μ_a leading to damped oscillations, a far larger region of plausible b and μ_a values predicts sustained oscillations. The uncertainty stems primarily from the parameter b (see univariate confidence intervals, Table 1). In future experiments, the value of b (larvae recruitment) could be estimated independently with more precision. Note that we withheld data from nine additional populations (three treatments, three replicates per treatment) from the parameter estimation process, in order to evaluate the predictive capabilities of the model (see *Model evaluation: demographically perturbed replicates* section). Including the nine additional time series in the ML estimates narrows considerably the confidence intervals for all the model parameters.

Model evaluation: control replicates

Is the noise structure assumed in the stochastic LPA model (Eqs. 16–18) adequate? Table 2 displays results of analyzing residuals of the combined model ("all,"

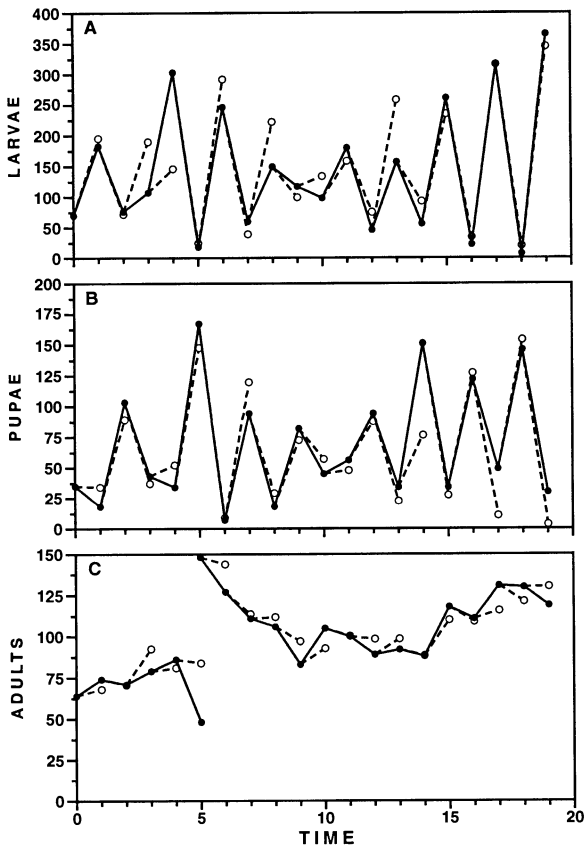

FIG. 14. Time series data (●) and one-step forecasts (○) for replicate B of Desharnais and Liu (1987) where 100 adults were added at $t = 5$. Solid lines connect the observed census data. The one-step forecasts (dashed-line projections) are based on the parameter estimates obtained from the control cultures.

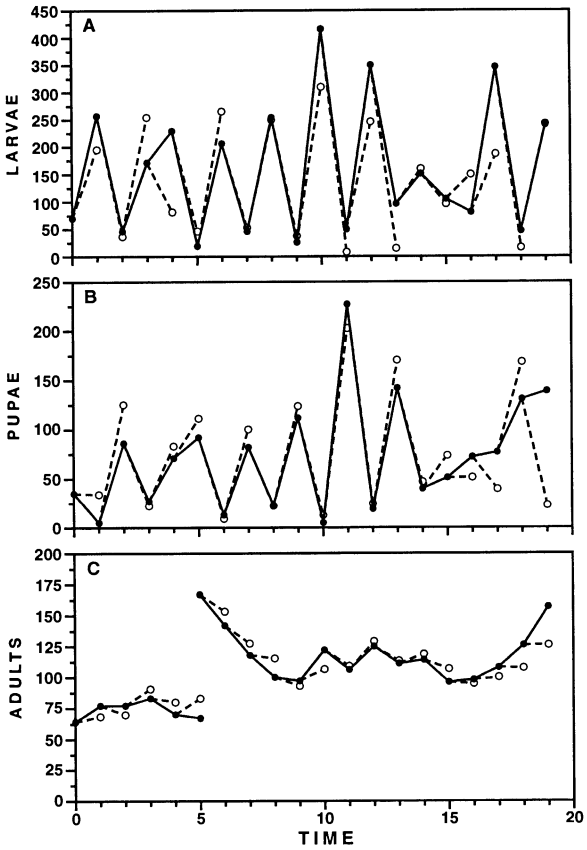

FIG. 15. Time series data (●) and one-step forecasts (○) for replicate C of Desharnais and Liu (1987) where 100 adults were added at $t = 5$. Solid lines connect the observed census data. The one-step forecasts (dashed-line projections) are based on the parameter estimates obtained from the control cultures.

Table 1) for univariate normality. First- and second-order autocorrelations and the Lin-Mudholkar normality statistic were calculated for each state variable in each of the replicates (A, B, C, D) used to estimate parameters. Replicate B revealed some second-order autocorrelation, but no first-order autocorrelation. Mild normality departure is displayed by the pupae of replicates A and C, and the adults of replicate C (Table 2).

Overall, the residuals conform adequately to the univariate normal model. Quantile-quantile (Q-Q) plots of the logarithmic residuals for larvae, pupae, and adults (Fig. 11A–C) reveal that the departures from normality indicated in Table 1 are due to a small number of outliers. In Fig. 11D, the multivariate normal residuals (quadratic forms, Eq. 35) are displayed in a chi-square Q-Q plot. The multivariate normal model describes the data reasonably well, except for four outliers (the four points on the extreme right of Fig. 11D). The four outliers (replicate A, $t = 1$; replicate B, $t = 1$; replicate B, $t = 17$; replicate C, $t = 5$) are evident in the original data and one-step plots (Figs. 7–10). As noted earlier, the deterministic LPA model can be viewed as a response surface representing the expected value of the logarithm of larval, pupal, and adult numbers at time $t + 1$ given the values of these variables at time t (Eqs. 20–22). The differences between the observed and model-predicted number of animals (residuals) are graphed in Fig. 12. The overall magnitude of the deviations is not large; furthermore, the residuals do not seem to vary systematically with the sizes of the state variables.

Model evaluation: demographically perturbed replicates

Can the model successfully forecast larval, pupal, and adult numbers for populations that were not used to estimate the parameters? One-step predictions, based on the parameter values obtained from the control cultures (Table 1), are compared with the observed time series data for nine demographically perturbed populations in Figs. 13–21. In the first treatment, 100 adults were added to each of the three cultures following the census at week 10 ($t = 5$). The model (Figs. 13–15)

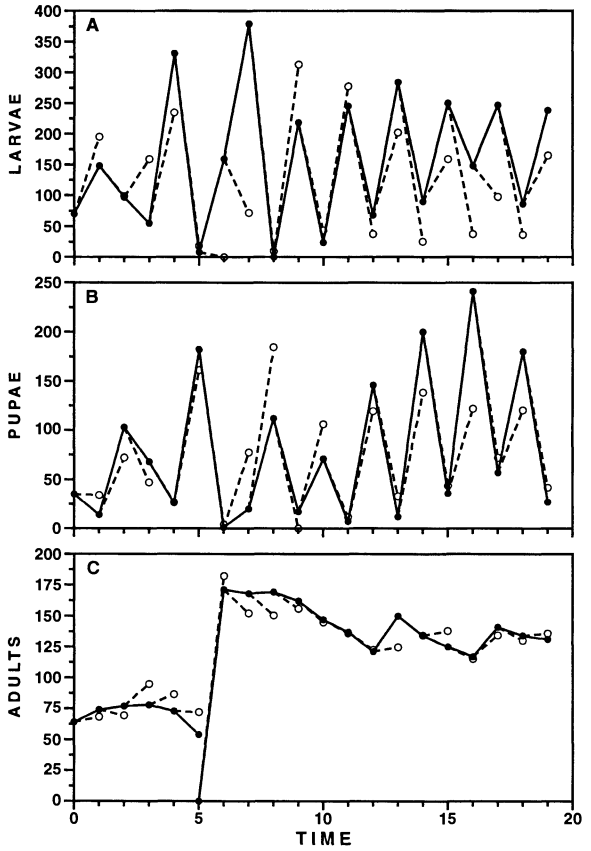

FIG. 16. Time series data (●) and one-step forecasts (○) for replicate A of Desharnais and Liu (1987) where all adults were removed at $t = 5$. Solid lines connect the observed census data. The one-step forecasts (dashed-line projections) are based on the parameter estimates obtained from the control cultures.

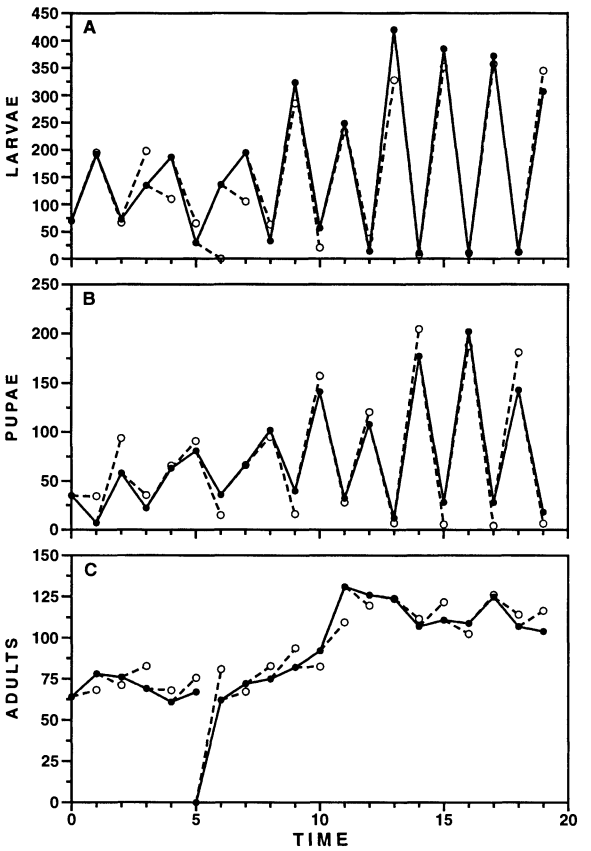

FIG. 17. Time series data (●) and one-step forecasts (○) for replicate B of Desharnais and Liu (1987) where all adults were removed at $t = 5$. Solid lines connect the observed census data. The one-step forecasts (dashed-line projections) are based on the parameter estimates obtained from the control cultures.

appears to handle the added adults quite adequately. In the second treatment, all of the adults were removed after the week 10 census. The predicted number of adults at week 12 ($t = 6$) are in agreement with the observed numbers (Figs. 16–18). The forecasts of larval numbers at week 12 are not good; removing all adults means that the model predicts no larvae at week 12, but larvae were observed. While the experimenters did remove adults they did not remove the eggs laid by those adults, consequently, larvae were observed at the next census. After this inconsistency between mathematical model and experimental protocol, the model recovers to make accurate population forecasts for $t \geq 8$. In the third treatment, all of the immature life stages (eggs, larvae, pupae) were removed (Figs. 19–21). The biology suggests a cascade of effects will follow. First, larval numbers at time $t + 1$ will be solely a function of adult numbers at time t. Second, no pupae will be observed at time $t + 1$, but this class will be present at $t + 2$. Finally, adult numbers at time $t + 3$ (6 wk following the removal of immatures) will increase. Each of these events are realized and the model successfully predicts each event both qualitatively and quantitatively. The ability of the model to reflect the behavior of the demographically perturbed populations gives us added confidence that the deterministic equations (Eqs. 1–3) capture the essential dynamical relationships among the state variables.

The prediction error analyses for each of the demographic treatments are summarized in Table 3. In the adults-added treatment, replicate A shows second-order autocorrelation by the larvae but no first-order autocorrelation, and replicate C reveals some first-order autocorrelation by adults. In the adults-removed treatment, replicate B shows some second-order autocorrelation by pupae. Departure from normality is displayed in 10 of the 27 treatment time series: by pupae (replicate B) and adults (replicates A, B) in the adults-added treatment, by larvae (replicates B, C) and pupae (replicate A) in the adults-removed treatment, and by larvae (replicate C), pupae (replicate A, C), and adults (replicate C) of the immatures-removed treatment. The normality departures are mostly moderate and can be traced to a small number of outliers in each time series.

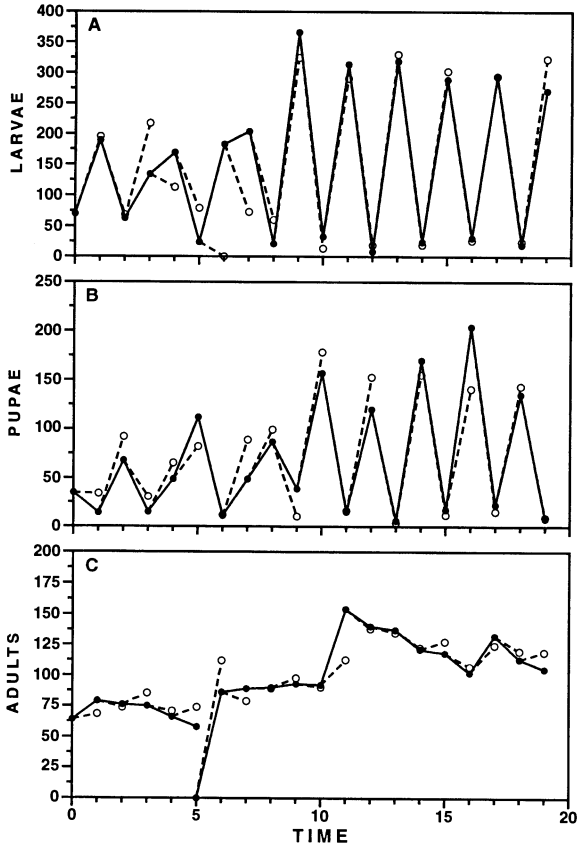

FIG. 18. Time series data (●) and one-step forecasts (○) for replicate C of Desharnais and Liu (1987) where all adults were removed at $t = 5$. Solid lines connect the observed census data. The one-step forecasts (dashed-line projections) are based on the parameter estimates obtained from the control cultures.

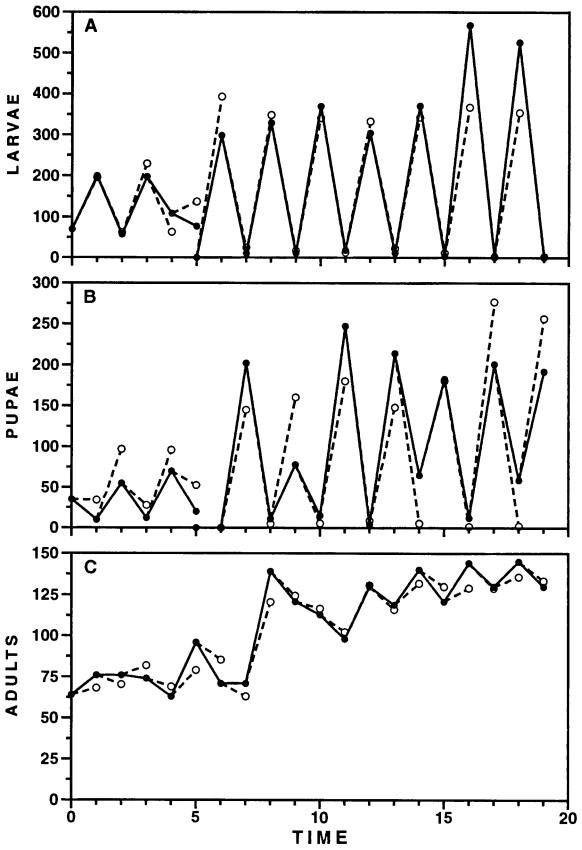

FIG. 19. Time series data (●) and one-step forecasts (○) for replicate A of Desharnais and Liu (1987) where all immatures were removed at $t = 5$. Solid lines connect the observed census data. The one-step forecasts (dashed-line projections) are based on the parameter estimates obtained from the control cultures.

Recall that these are prediction error analyses, rather than analyses of residuals as in Table 2, since these cultures were not part of the parameter estimation process. Overall, the predictions support the stochastic LPA model.

DISCUSSION

The role of nonlinear demographic theory in ecology will ultimately be decided by tests with experimental data. If demographic models cannot yield quantitative predictions in well-studied laboratory and field systems, it is unlikely that such models will yield convincing qualitative insights into any other ecological systems. The *Tribolium* system has been studied extensively for over 60 yr and is a prime candidate for an attempt at a detailed mathematical understanding.

Locating populations in model parameter space

Consistent with earlier work (Chapman 1928, Landahl 1955, Taylor 1965, Desharnais and Costantino 1985, Hastings and Costantino 1987, 1991, Costantino and Desharnais 1991), we accept the hypothesis that the fluctuations in animal numbers observed in laboratory populations of beetles are due primarily to the nonlinear cannibalistic interactions among eggs, larvae, pupae, and adults. We arrive at this conclusion in the following way: first, by writing an explicit three-state-variable demographic model incorporating the major factors of the population biology of the beetle (specifically, birth, death, and cannibalism); second, by mathematical and numerical analyses of the model's dynamics; third, by incorporating a stochastic component in the model that provides an explicit likelihood function for estimating parameters from time series data; and fourth, by evaluating the full stochastic model using an independent data set and using statistical diagnostic methods based on an analysis of residuals (one-step forecast errors). Culmination of this four-step process allows us to estimate the location of the populations in parameter space (Fig. 3). Specifically, for the data set studied here (Desharnais and Costantino 1980) the populations are placed in the region of parameter space that corresponds to stable 2-cycles.

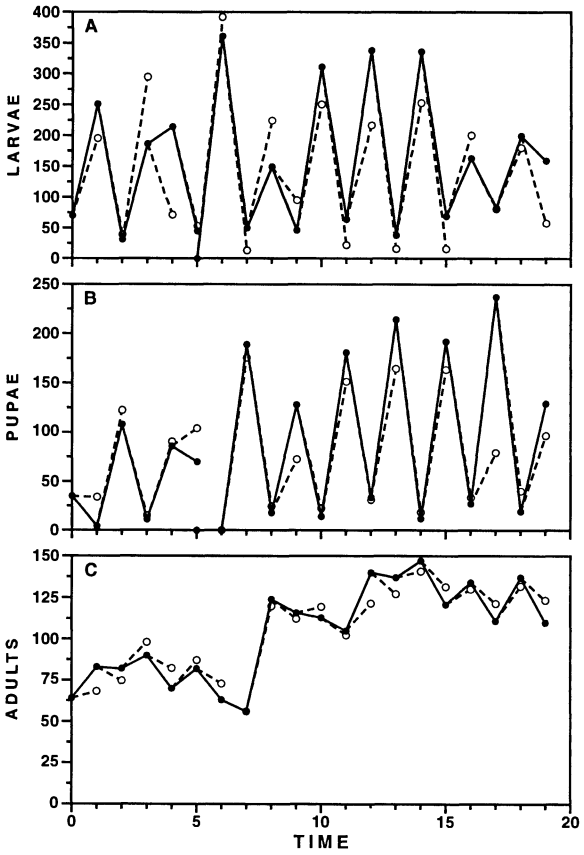

FIG. 20. Time series data (●) and one-step forecasts (○) for replicate B of Desharnais and Liu (1987) where all immatures were removed at $t = 5$. Solid lines connect the observed census data. The one-step forecasts (dashed-line projections) are based on the parameter estimates obtained from the control cultures.

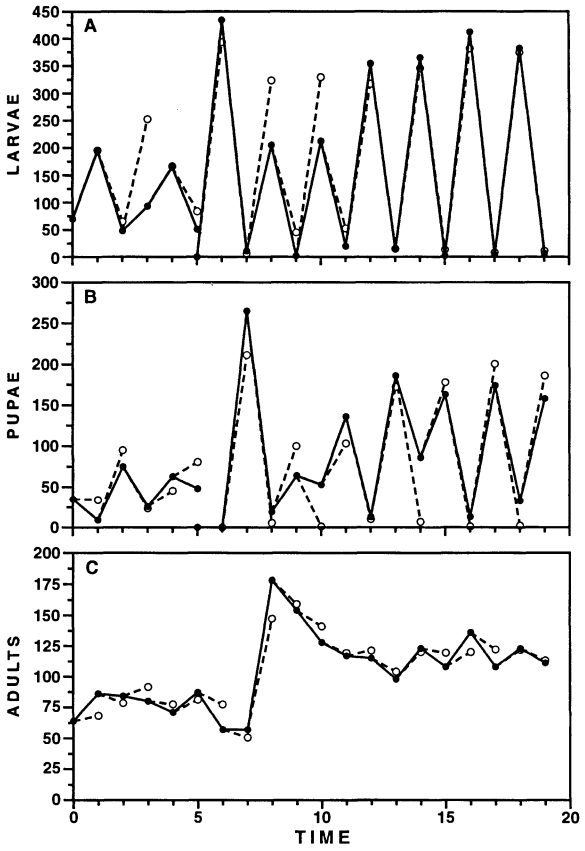

FIG. 21. Time series data (●) and one-step forecasts (○) for replicate C of Desharnais and Liu (1987) where all immatures were removed at $t = 5$. Solid lines connect the observed census data. The one-step forecasts (dashed-line projections) are based on the parameter estimates obtained from the control cultures.

Stochastic realizations

In recent years, we have interpreted fluctuations in adult numbers as a stochastic equilibrium with a gamma stationary distribution (Costantino and Desharnais 1981, Dennis and Costantino 1988, Desharnais et al. 1990, Costantino and Desharnais 1991). Are the gamma model and the stochastic LPA model consistent with each other? The answer is yes, provided the underlying adult dynamics are either a stable point (Fig. 5B) or a stable cycle with oscillations of small magnitude (Fig. 5A). Fig. 22 depicts a frequency histogram of adult numbers simulated from the stochastic LPA model. The time series was generated using the parameter values estimated from the laboratory populations ("all" in Table 1) and contains 1000 observations. As we have noted, the parameter values correspond to a 2-cycle of adult numbers. The histogram in Fig. 22 resembles a gamma probability distribution. The amplitude of the underlying 2-cycle fluctuations is small compared to the magnitude of the noise fluctuations and so the 2-cycle is not evident in the histogram. Clearly, stationary distributions provide limited information concerning the details of the fluctuations in animal numbers. On the other hand, these distributions do provide a very practical quantitative assessment of the frequency of occurrence of particular population sizes. The adult numbers behave like a population with a growth rate that has a stable equilibrium but is perturbed by environmental noise, precisely the conditions that lead to a gamma-like stationary distribution of population abundance (Dennis and Patil 1984).

An important feature of our argument for the identification of the deterministic dynamics in the presence of stochasticity is that the three-variable stochastic model allowed us to quantify the relative contribution of the stochastic component. The model diagnostic techniques used evaluate explicitly whether the assumed random element adequately describes the data. By incorporating a testable stochastic component into the model we are able to discern stable 2-cycle behavior.

New experiments

The ability to reliably locate populations in parameter space opens the possibilities for many new ex-

TABLE 3. Prediction error anlayses. First ($\hat{\rho}_1$) and second-order ($\hat{\rho}_2$) sample autocorrelations and Lin-Mudholkar (z) test statistic for normality, calculated for each of the three replicates (A, B, C) of three demographic perturbation treatments.

		Demographic perturbation treatment								
		Adults added			Adults removed			Immatures removed		
		A	B	C	A	B	C	A	B	C
L_t	$\hat{\rho}_1$	0.37	−0.43	−0.06	0.04	−0.16	−0.14	−0.14	−0.15	−0.11
	$\hat{\rho}_2$	0.59*	0.28	0.18	−0.17	−0.22	−0.28	−0.19	−0.20	−0.07
	z	1.23	−0.24	−0.71	0.15	−2.86**	−2.71**	1.50	−0.96	2.74**
P_t	$\hat{\rho}_1$	−0.38	−0.04	−0.01	−0.11	−0.08	0.14	−0.14	−0.24	−0.35
	$\hat{\rho}_2$	0.44	0.43	0.08	−0.24	0.51*	−0.06	0.39	0.20	0.39
	z	−0.84	−2.72**	−0.11	−2.94**	−0.36	−1.16	−2.19**	1.67	−2.29**
A_t	$\hat{\rho}_1$	0.35	−0.01	0.51*	0.38	0.21	0.21	−0.39	0.23	−0.01
	$\hat{\rho}_2$	0.19	0.07	0.08	−0.09	−0.11	−0.11	−0.14	0.03	−0.11
	z	2.57**	2.65**	−0.46	1.52	0.09	−0.67	0.27	−0.46	−3.77**

* Significant (0.05 level of probability) j^{th} order autocorrelation if $|\hat{\rho}_j|$ exceeds 0.46.
** Significant (0.05 level of probability) departure from normality if $|z|$ exceeds 1.96.

periments. The modern theory of nonlinear dynamics (i.e., bifurcation theory) provides guidance for the conduct of a new phase of population research in which the rigorous statistical verification of experimentally designed shifts in dynamical behavior would provide convincing evidence for the relevance of nonlinear mathematics in population ecology, including the possibility of chaos. For example, on the basis of Fig. 3, which was generated from a historical data set, experimentally increasing the rate of adult mortality should result in the disappearance of the oscillations in animal numbers: the dynamics change from a 2-cycle to a stable fixed-point attractor. With an additional increase in adult mortality we expect aperiodic, "chaos-like" fluctuations in animal numbers. By applying our approach we should be able to document predicted transitions in dynamical behavior including transitions to chaos.

CONCLUDING REMARKS

The prospect of identifying nonlinear demographic behaviors in ecological systems continues to provoke debate. Ecologists are comfortable with the assertion that nonlinear systems can display limit cycles, multiple attractors, and strange attractors, because the assertion is a mathematical fact. Ecologists for the most part also agree that ecological relationships are frequently, perhaps largely, nonlinear. Particular nonlinear behaviors, however, are tantalizingly difficult to pin to any given, real ecological system. Ecological systems are complex: alternate explanations abound; data collection is challenging; noise is prevalent. Are periodic fluctuations observed in a system really limit cycles caused by some intrinsic, identifiable mechanism, or are they caused by some unobserved external forces? Did a system get pushed into a different attractor, or have conditions assumed by the model simply changed? Is it chaos or is it noise?

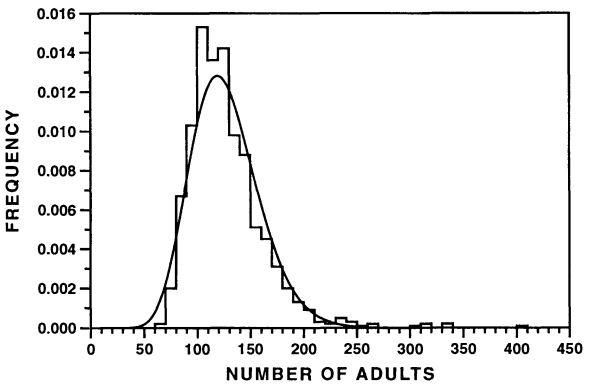

FIG. 22. Histogram of adult numbers for the stochastic LPA model simulated for 1000 time steps using the parameter values (Table 1) and variance-covariance matrix estimated from the control cultures. The smooth curve represents a gamma probability density function fitted to the stochastic realizations.

We believe that part of the difficulty stems from lack of explicit connections between models and data, between theories and experiments. First, theoretical models in ecology tend to emphasize qualitative dynamics. The end product of an investigation is a broad map of the phase-parameter space of a simplified deterministic model, with the delimited regions governed by different types of attractors. We presented such a study, of a three-variable difference equation model of *Tribolium* life stages, in the second section of this paper. Because of the highly nonlinear interactions of cannibalism, the model has it all: extinction, stable points, periodic cycles, aperiodic orbits, multiple attractors, and strange attractors. Second, the laboratory or field data tend to be collected for reasons other than testing a specific mathematical model. Data are precious, models are cheap. A well-designed empirical study often answers many questions and rules out many models. That a previous *Tribolium* experiment provided, for our particular model, data for parameter estimates and separate data for model evaluation, was a fortunate but incidental aspect of the experiment. Third, theoretical ecology has had a paradoxically weak statistical tradition. Even if model and data are in concert, the mathematical

ecology literature provides little guidance as to what to do with the data. The statistical interface between model and data that we reported here was helpful toward making theories more accountable to experiments.

ACKNOWLEDGMENTS

We thank Pauline Hackney for her skilled word processing assistance. This work was supported in part by U.S. National Science Foundation grants DMS-9206678, DMS-9306271, and DMS-9319073.

LITERATURE CITED

Bartlett, M. S. 1990. Chance or chaos? (with discussion.) Journal of the Royal Statistical Society **A52**:321–347.

Carpenter, S. R., K. L. Cottingham, and C. A. Stow. 1994. Fitting predator-prey models to time series with observation errors. Ecology **75**:1254–1264.

Caswell, H. 1989. Matrix population models. Sinauer, Sunderland, Massachusetts, USA.

Chapman, R. N. 1928. Quantitative analysis of environmental factors. Ecology **9**:111–122.

Costantino, R. F., and R. A. Desharnais. 1981. Gamma distributions of adult numbers for *Tribolium* populations in the region of their steady states. Journal of Animal Ecology **50**:667–681.

Costantino, R. F., and R. A. Desharnais. 1991. Population dynamics and the *Tribolium* model: genetics and demography. Springer-Verlag, New York, New York, USA.

Cox, D. R., and N. J. H. Small. 1978. Testing multivariate normality. Biometrika **65**:263–272.

Cushing, J. M. 1988. Nonlinear matrix models and population dynamics. Natural Resource Modeling **2**:539–580.

Dennis, B., and R. F. Costantino. 1988. Analysis of steady-state populations with the gamma abundance model: application to *Tribolium*. Ecology **69**:1200–1213.

Dennis, B., P. L. Munholland, and J. M. Scott. 1991. Estimation of growth and extinction parameters for endangered species. Ecological Monographs **61**:115–143.

Dennis, B., and G. P. Patil. 1984. The gamma distribution and weighted multimodal gamma distributions as models of population abundance. Mathematical Biosciences **68**: 187–212.

Desharnais, R. A., and R. F. Costantino. 1980. Genetic analysis of a population of *Tribolium*. VII. Stability: response to genetic and demographic perturbations. Canadian Journal of Genetics and Cytology **22**:577–589.

Desharnais, R. A., and R. F. Costantino. 1985. Genetic analysis of a population of *Tribolium*. VIII. The stationary stochastic dynamics of adult numbers. Canadian Journal of Genetics and Cytology **27**:341–350.

Desharnais, R. A., B. Dennis, and R. F. Costantino. 1990. Genetic analysis of a population of *Tribolium*. IX. Maximization of population size and the concept of a stochastic equilibrium. Genome **33**:389–400.

Desharnais, R. A., and L. Liu. 1987. Stable demographic limit cycles in laboratory populations of *Tribolium castaneum*. Journal of Animal Ecology **56**:885–906.

Ellner, S., A. R. Gallant, D. McCaffrey, and D. W. Nychka. 1991. Convergence rates and data requirements for Jacobian-based estimates of Lyapunov exponents from data. Physical Letters **153**:357–363.

Hastings, A., and R. F. Costantino. 1987. Cannibalistic egg-larva interaction in *Tribolium*: an explanation for the oscillations in population numbers. American Naturalist **130**: 36–52.

Hastings, A., and R. F. Costantino. 1991. Oscillations in population numbers: age-dependent cannibalism. Journal of Animal Ecology **60**:471–482.

Hastings, A., C. L. Hom, S. Ellner, P. Turchin, and H. C. J. Godfray. 1993. Chaos in ecology: is mother nature a strange attractor? Annual Review of Ecology and Systematics **24**:1–33.

Hilborn, R., and C. J. Walters. 1992. Quantitative fisheries stock assessment. Chapman and Hall, New York, New York, USA.

Klimko, L. A., and P. I. Nelson. 1978. On conditional least squares estimation for stochastic processes. Annals of Statistics **6**:629–642.

Landahl, H. D. 1955. A mathematical model for the temporal pattern of a population structure, with a particular reference to the flour beetle. Bulletin of Mathematical Biophysics **17**: 63–77.

Lankshmikantham, V., and D. Trigiante. 1988. Theory of difference equations: numerical methods and applications. Mathematics in science and engineering. Volume 181. Academic Press, New York, New York, USA.

Leslie, P. H. 1948. Some further notes on the use of matrices in population mathematics. Biometrika **35**:213–245.

Lin, C. C., and G. S. Mudholkar. 1980. A simple test for normality against asymmetric alternatives. Biometrika **67**: 455–461.

Logan, J. A., and J. C. Allen. 1992. Nonlinear dynamics and chaos in insect populations. Annual Review of Entomology **37**:455–477.

Logan, J. A., and F. P. Hain. 1991. Chaos and insect ecology. Virginia Experiment Station Information Series 91-3. Virginia Polytechnic Institute and State University, Blacksburg, Virginia, USA.

Ludwig, D., and C. J. Walters. 1989. A robust method for parameter estimation from catch and effort data. Canadian Journal of Fisheries and Aquatic Sciences **46**:137–144.

May, R. M. 1974*a*. Biological populations with nonoverlapping generations: stable points, stable cycles and chaos. Science **186**:645–647.

———. 1974*b*. Stability and complexity in model ecosystems. Second edition. Princeton University Press, Princeton, New Jersey, USA.

McCaffrey, D. F., S. Ellner, A. R. Gallant, and D. W. Nychka. 1992. Estimating the Lyapunov exponent of a chaotic system with a nonparametric regression. Journal of the American Statistical Association **87**:682–695.

McCullagh, P., and J. A. Nelder. 1989. Generalized linear models. Second edition. Chapman and Hall, London, England.

Moffa, A. M., and R. F. Costantino. 1977. Genetic analysis of a population of *Tribolium*. VI. Polymorphism and demographic equilibrium. Genetics **87**:785–805.

Olsson, D. M., and L. S. Nelson. 1975. The Nelder-Mead simplex procedure for function minimization. Technometrics **17**:45–51.

Park, T., D. B. Mertz, W. Grodzinski, and T. Prus. 1965. Cannibalistic predation in populations of flour beetles. Physiological Zoology **38**:289–321.

Press, W. H., B. P. Flannery, S. A. Teukolsky, and W. T. Vetterling. 1986. Numerical recipes: the art of scientific computing. Cambridge University Press, Cambridge, England.

Schaffer, W. M. 1984. Stretching and folding in lynx fur returns: evidence for a strange attractor in nature. American Naturalist **124**:798–820.

———. 1985. Order and chaos in ecological systems. Ecology **66**:93–106.

Schaffer, W. M., and M. Kot. 1985. Do strange attractors govern ecological systems? BioScience **35**:342–350.

Schaffer, W. M., and M. Kot. 1986*a*. Differential systems in ecology and epidemiology. Pages 158–178 *in* A. V. Holden, editor. Chaos. Princeton University Press, Princeton, New Jersey, USA.

Schaffer, W. M., and M. Kot. 1986*b*. Chaos in ecological

systems: the coals that Newcastle forgot. Trends in Ecology and Evolution **1**:58–63.

Seber, G. A. F. 1984. Multivariate observations. John Wiley & Sons, New York, New York, USA.

Shaffer, M. L. 1981. Minimum population sizes for species conservation. BioScience **31**:131–134.

Simberloff, D. 1988. The contribution of population and community ecology to conservation science. Annual Review of Ecology and Systematics **19**:473–511.

Sokoloff, A. 1974. The biology of *Tribolium*. Volume 2. Oxford University Press, Oxford, England.

Stuart, A., and J. K. Ord. 1991. Kendall's advanced theory of statistics. Volume 2: classical inference and relationships. Fifth edition. Griffin, London, England.

Takens, F. 1980. Detecting strange attractors in turbulence. *In* D. A. Rand and L.-S. Young, editors. Dynamical systems and turbulence. Lecture Notes in Mathematics **898**:366–381.

Taylor, N. W. 1965. A theoretical study of population regulation in *Tribolium confusum*. Ecology **46**:334–340.

Tong, H. 1990. Nonlinear time series: a dynamical system approach. Oxford University Press, Oxford, England.

Turchin, P. 1993. Chaos and stability in rodent population dynamics: evidence from nonlinear time-series analysis. Oikos **68**:167–172.

Turchin, P., and A. D. Taylor. 1992. Complex dynamics in ecological time series. Ecology **73**:289–305.

Venzon, D. J., and S. H. Moolgavkar. 1988. A method for computing profile-likelihood-based confidence intervals. Applied Statistics **37**:87–94.